# The Yellow Dog Peridotite & a Possible Buried Igneous Complex of Lower Keweenawan Age in the Northern Peninsula of Michigan

Geological Survey
Michigan DNR
Report of
Investigation 24


Geological Survey Division

---

Report of Investigation 24

---

# THE YELLOW DOG PERIDOTITE AND A POSSIBLE BURIED IGNEOUS COMPLEX OF LOWER KEWEENAWAN AGE IN THE NORTHERN PENINSULA OF MICHIGAN

By

John S. Klasner, David W. Snider,
W. F. Cannon, and John F. Slack

Lansing, Michigan

1979

Published by authority of State of Michigan
Compiled Laws of 1970 section 321.6

---

Copies of this and all other Department of Natural Resources publications
are available from:

Information Services Center
Michigan Department of Natural Resources
Box 30028
Lansing, Michigan 48909

On deposit in many libraries in Michigan
and other selected locations

# PREFACE

This report is the result of a joint effort by the United States Geological Survey and the Geological Survey Division, Michigan Department of Natural Resources. Specific units involved in the project were the Eastern Mineral Resources Branch of the U.S. Geological Survey and the Geology and Minerals Research Unit, Michigan Geological Survey.

Both agencies became interested in a somewhat anomalous peridotite body outcropping in an otherwise flat sand plain in northern Marquette County, Michigan. Discussions between the two agencies culminated in an agreement to combine efforts in a thorough investigation of this curious rock body.

The report presents the multidisciplinary approach of geology, geochemistry and geophysics to the problem. The use of such an approach has proven to produce more scientifically complete results than would have been possible with a single discipline. In addition, the study has been extremely cost-efficient.

David W. Snider, Geologist
Geology & Minerals Research Unit
Geological Survey Division
Michigan Department of Natural
Resources
Lansing, Michigan 48909

CONTENTS

ILLUSTRATIONS

Figures



Tables

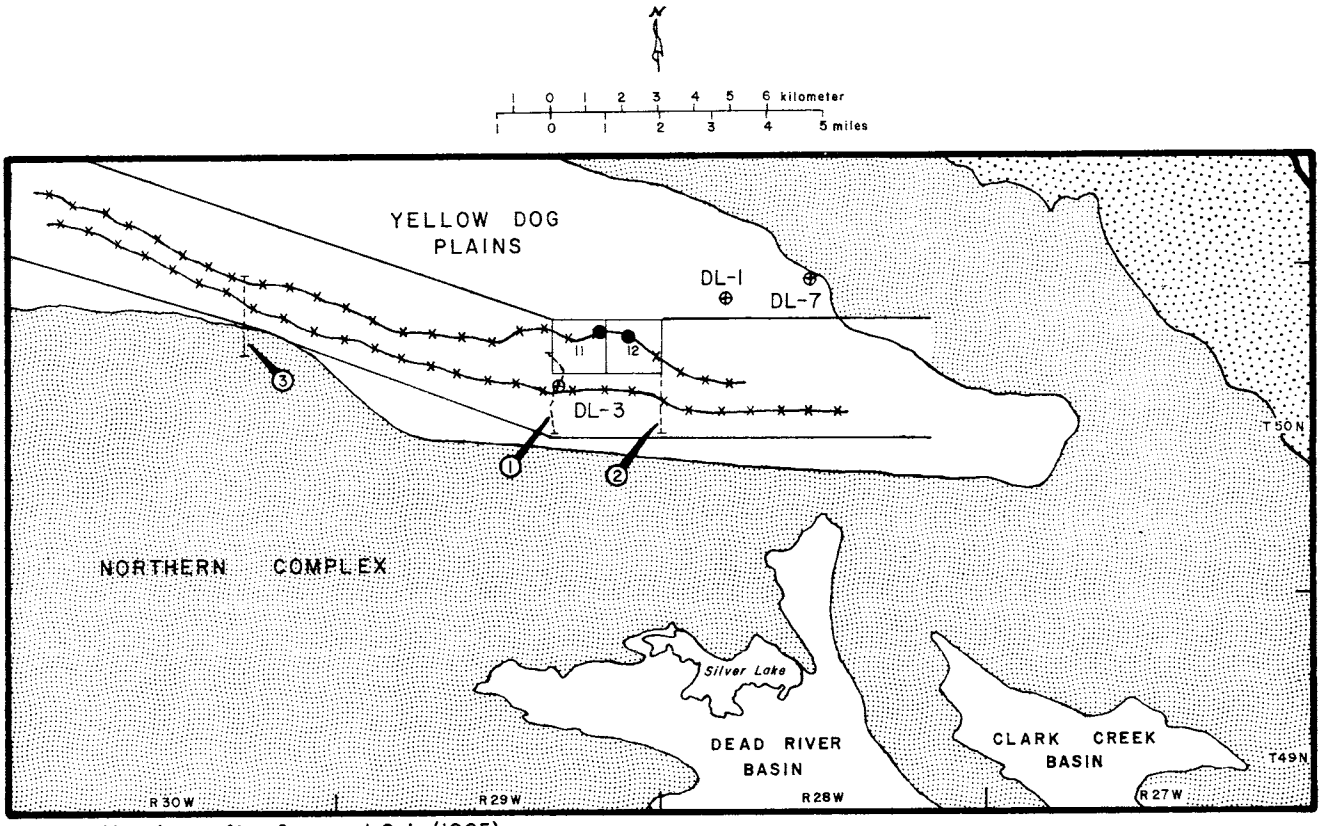


Map base after Case and Gair (1965).

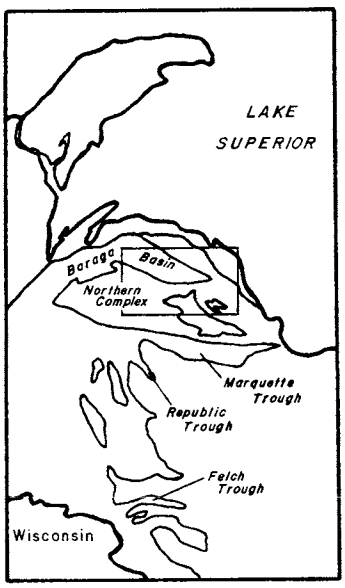



EXPLANATION

① Location of regional geophysical lines

① VLF-EM, gravity, ground magnetics

② gravity, ground magnetics

③ VLF-EM, ground magnetics

Location of two regional aeromagnetic anomalies

General location of outcrops

Location of regional ground magnetic survey

Location of drill holes. See Trow, 1978 for detailed descriptions.

Precambrian Y rocks

Precambrian X rocks

Precambrian W rocks

Figure 1. Yellow Dog Plains general regional geology and location.

# THE YELLOW DOG PERIDOTITE AND A POSSIBLE BURIED IGNEOUS COMPLEX OF LOWER KEWEENAWAN AGE IN THE NORTHERN PENINSULA OF MICHIGAN

By

John S. Klasner[1], David W. Snider[2],
W. F. Cannon[1], and John F. Slack[1]

## Abstract

Partly serpentinized peridotite of early Keweenawan age crops out in two places along a 20-kilometer-long zone of positive aeromagnetic anomalies in northern Marquette County, Michigan. Most of the area is mantled by Pleistocene drift with few bedrock exposures.

Petrographic and electron microprobe studies show that the peridotite was originally a plagioclase lherzolite containing 40 to 50 percent olivine ($Fo_{80}$) and approximately 10 to 15 percent each of enstatite ($En_{78}Wo_{04}Fs_{18}$) and diopsidic augite ($En_{47}Wo_{42}Fs_{11}$). The plagioclase varies from 5 to 10 percent, and according to Morris (1977) is labradorite, with a composition of $An_{57-65}$. Major oxide minerals (4 to 6 percent) are ilmenite and magnetite. Sulfides comprise 1 to 2 percent of the peridotite and are chiefly pyrrhotite, pentlandite, and chalcopyrite.

Ground magnetic, gravity, and very low frequency electro-magnetic (VLF-EM) surveys have refined the location and magnitude of anomalies previously known only from aeromagnetic studies. These surveys together with soil geochemical studies suggest that peridotite, and possibly other mafic rocks forming a differentiated igneous complex, may occur throughout a belt 20 kilometers long (east-west) and 1 to 2 kilometers wide (north-south).

Differentiated igneous complexes in many parts of the world are hosts for copper, nickel, chromium, or precious-metal deposits. The peridotite in the area of this study is anomalously rich in copper and sulfur compared to world-wide averages for peridotite. Positive electro-magnetic anomalies found near the peridotite outcrops may be caused by sulfide-rich zones in the igneous rocks and should be explored further for copper-nickel mineralization.

## INTRODUCTION

The Yellow Dog Plains in northern Marquette County, Michigan, is a nearly featureless area covered by Pleistocene sand and gravel and is nearly devoid of bedrock exposures. The bedrock beneath the plains is mostly slate and other metasedimentary rock of the Michigamme Formation and has been shown as such on virtually all geologic compilations of the region. However, in Sections 11 and 12, T50N, R29W, there are two outcrops of massive, partly serpentinized peridotite. The outcrops lie on and form the highest magnetic peaks of a west-trending linear aeromagnetic anomaly which is about 20 kilometers long (see Figure 1). The anomaly lies parallel to another anomaly of comparable magnitude about 0.5 to 1 kilometer to the south. Both anomalies appear to cut the regional structural trends at low angles.

The two anomalies were first evaluated by Case and Gair (1965) and were inferred by them to be caused by magnetic sedimentary units in the Michigamme Formation. At that time, the existence of the peridotite outcrops was not generally known. Because of the close association of the peridotite outcrops with the observed aeromagnetic anomalies and because the anomalies appear to cut across structural trends in the Michigamme Formation, we believe that both anomalies are associated with peridotite.

The relatively fresh, undeformed nature of the peridotite suggests that it is younger than the Penokean orogeny which deformed and metamorphosed other rocks in the area about 1.9 billion years ago. Because komatiitic magmas are not common in rocks younger than about 2.5 billion years and because the texture and chemical composition of the peridotite suggest that it is a crystal cumulate, we estimate it is more likely that the peridotite is a differentiate from a less mafic magma rather than a product of a parental ultramafic magma.

1/ U. S. Geological Survey, Reston, Virginia

2/ Geological Survey Division, Michigan Department of Natural Resources, Lansing, Michigan

The present study was undertaken to determine if a relatively large differentiated igneous complex is beneath the Yellow Dog Plains and, if so, to determine its configuration and potential economic mineralization. An integrated program including ground magnetic, very low frequency electromagnetic (VLF-EM), gravity, paleomagnetic, rock chemistry and mineralogy, and soil chemistry studies was carried out in 1976 as a cooperative project between the U. S. Geological Survey, Eastern Mineral Resources Branch and the Geology and Minerals Research Unit of the Geological Survey Division, Michigan Department of Natural Resources. This report presents the results of that study and our inferences of the geology and mineral resource potential of the area of the Yellow Dog Peridotite and associated anomalies.

Ackowledgments. R. Lilienthal, P. Geraci, and A. Grosz performed much of the geophysical field work, data reduction, and plotting. S. Quam assisted in interpreting and modeling the gravity data. Kenneth Books performed the magnetic susceptibility and remanence studies. L. B. Wiggins assisted in the microprobe analyses. M. P. Foose reviewed the manuscript. Michigan Geological Survey Division personnel were instrumental in bringing the report to final form for publication. Final editing was accomplished by Beverly L. Champion; layout, graphics and word processing were coordinated by Steven E. Wilson; drafting by Darrell Hodge and Gregory A. Wilson; and manuscript typing by Lois J. DeClaire.

## GENERAL GEOLOGY

The region surrounding the Yellow Dog Peridotite contains Precambrian rocks of three ages. A gneiss-greenstone complex older than 2.5 billion years (Precambrian W) forms the basement for roughly 2 -billion-year-old (Precambrian X) rocks of the Marquette Range Supergroup. The Marquette Range Supergroup is preserved in grabens of Precambrian W rocks formed during the Penokean orogeny about 1.9 billion years ago (Cannon, 1973). Figure 1 shows the aerial distribution of Precambrian W, X and Y rocks near Yellow Dog Plains. The plains, formed of Pleistocene sand and gravel, are underlain mostly by the Michigamme Formation, part of the Marquette Range Supergroup, in a structural trough known informally as the Baraga Basin. They are flanked by Precambrian W gneiss and greenstone on the north, east, and south. Because of the extensive Pleistocene cover in the basin, little is known of the nature of the Michigamme Formation. Most exposures are along the southern flank of the basin where basal conglomerate, quartzite, and arkose as much as 20 meters thick underly black slate and argillite. The Michigamme beneath the study area consists of fine-grained clastic rocks, largely black slate and argillite as shown by recent drilling (Trow, 1978 a,b,c). These rocks were deformed and metamorphosed to the greenschist facies about 1.9 billion years ago, during the Penokean orogeny.

The third age of Precambrian rocks is represented by west-trending diabase dikes of early Keweenawan age. The dikes were intruded and cooled during a period of reversed magnetic polarity about 1.1 billion years ago (Precambrian Y). Their negative remanent magnetization produces pronounced linear magnetic lows over the dikes and allows them to be identified and traced with certainty on aeromagnetic maps.

The Yellow Dog Peridotite is known from two exposures (see Figure 1). Because it is undeformed and only moderately serpentinized, it was judged from field evidence to be younger than the Penokean orogeny that deformed and metamorphosed the surrounding Precambrian W and X rocks into which the peridotite was emplaced. Because the peridotite causes prominent positive aeromagnetic anomalies, it was initially believed that it was not related to lower Keweenawan diabase dikes that typically produce magnetic lows. Subsequent paleomagnetic studies by Kenneth Books of the U.S. Geological Survey, however, confirm that when the soft components of remanent magnetization are removed the peridotite does have a reversed remanent pole position very similar to that of other lower Keweenawan rocks in the region.

## PETROLOGY

### Texture, Mineralogy and Bulk Composition

The peridotite is reddish brown on weathered surfaces and greenish black on fresh surfaces. The weathered rind is generally confined to a few millimeters of the surface. The rock is massive and coarse grained, without visible layering, banding, or foliation. Poikilitic pyroxene is commonly a centimeter or more in length; olivine generally is 2 to 5 millimeters in diameter.

Microscopic examination indicates that the rock was originally a plagioclase lherzolite containing 40 to 50 percent olivine (now from 1/2 to 2/3 replaced by serpentine) and 20 to 30 percent pyroxene, with clinopyroxene generally slightly more abundant than orthopyroxene. Plagioclase comprises about 5 to 10 percent of the rock, and chlorite is present in amounts ranging from 5 to 15 percent. Opaque minerals, discussed in more detail below, make up 5 to 8 percent. A variety of other minerals including both brown and green amphibole, red-brown biotite, sericite, talc, carbonate, clinozoisite, and rare colorless spinel (?) together comprise 5 to 10 percent of the rock.

Olivine occurs as euhedral phenocrysts, now partly altered to serpentine. Adjacent euhedral phenocrysts commonly are in contact with each other and appear to be accumulations of crystals that have settled from the magma rather than crystals that have grown in place, since there is no indication that the shape of the olivine grains is controlled by contact with adjacent grains.

Olivine phenocrysts typically are surrounded by subhedral to anhedral pyroxene varying from about the same size as olivines to large grains poikilitically enclosing olivine phenocrysts. Some orthopyroxenes are euhedral, however, indicating crystal growth contemporaneous with olivine. Plagioclase generally occurs as subhedral and anhedral grains interstitial to pyroxene crystals. In a few places, it forms euhedral laths entirely within orthopyroxene, suggesting crystallization of at least some plagioclase prior to both pyroxene types. Green amphibole (actinolite) occurs as an alteration product of clinopyroxene and is clearly secondary. Brown hornblende forms rims on pyroxene grains and locally exhibits intercumulus textures suggesting a primary origin. Biotite occurs chiefly as subhedral laths which in places poikilitically enclose euhedral olivine. Most appears to have formed as an alteration of pyroxene, although the genesis of some euhedral intercumulus grains is not clear.

No cataclastic textures or other metamorphic fabrics are present on a microscopic scale. Minor deformation is displayed by shattered plagioclase grains and bent and kinked biotite flakes. The deformation may be due to volume expansion during the serpentinization of olivine (i.e., Hostetler et al, 1966; Coleman and Keith, 1971). Commonly, the shattering of plagioclase is most intense where crystal terminations of serpentinized olivine grains impinge on plagioclase grains.

The origin of the peridotite is important in assessing the potential for contained mineral deposits. Economic copper, nickel, and precious-metal ores are characteristically associated with layered mafic or ultramafic intrusions (i.e., Sudbury, Duluth), rather than with alpine-type intrusions. Utilizing criteria outlined by Thayer (1960), the Yellow Dog Peridotite displays textural and mineralogical features strongly suggestive of a stratiform mafic-ultramafic genesis. If it is a product of a parental ultramafic magma (a komatiite), it might contain nickel sulfide deposits. If, on the other hand, it is a differentiate from a less mafic magma, disseminated copper-nickel sulfides, chromite, or precious-metal ores could be present. The chemical composition of the peridotite (Table 1) suggests that the rock is not a komatiite and that the present composition more likely is a result of differentiation from basaltic magma. Specifically, the high $TiO_2$/MgO ratio, and the low $Al_2O_3$ content for a corresponding FeO/FeO+MgO ratio shown by the peridotite are more characteristic of a tholeiite than of a komatiite, according to data summarized by Naldrett and Cabri (1976) and Arndt et al. (1977). This, together with the presence of cumulus olivine textures suggests that the bulk composition of the magma from which the peridotite crystallized was considerably less mafic than the present rock.

| | no. 6 | no. 35 |
|---|---|---|
| $SiO_2$ | 45.0 | 40.2 |
| $TiO_2$ | 0.83 | 0.92 |
| $Al_2O_3$ | 4.4 | 6.0 |
| $Fe_2O_3$ | 14.3 | 6.4 |
| FeO | (total Fe) | 7.7 |
| MnO | 0.18 | 0.18 |
| MgO | 24.9 | 24.9 |
| CaO | 4.4 | 3.1 |
| $Na_2O$ | 0.36 | 0.40 |
| $K_2O$ | 0.11 | 0.20 |
| $P_2O_5$ | 0.10 | 0.046 |
| F | na | 0.03 |
| LOI[1] | 5.56 | 7.8 |
| Moisture (at 105°C) | na | 0.01 |
| $CO_2$ | na | 0.1 |
| Total | 100.15 | 97.99 |

na - not analyzed

[1] LOI - loss on ignition at 1,000°C

no. 6 from the section 12 outcrop and was analyzed by the Rocky Mountain Geochemical Corporation

no. 35 from section 11 outcrop and was analyzed by Skyline Labs, Inc.

Table 1. Chemical analyses of the Yellow Dog Peridotite expressed in weight percent.

## Composition of Major Primary Silicate Minerals

Chemical analyses of olivines and pyroxenes were obtained with an ARL-EMX-SM electron microprobe operated at an accelerating potential of 15 KV and a beam current of 0.05 mA. Crystals used were ADP, LiF, and RAP, with 20-second counting intervals on 2 to 3 micron-sized spots. Data reduction was performed by the method of Bence and Albee (1968). Two samples from the Section 12 outcrop (Figure 2) were studied. Compositions in Tables 2 and 3 represent means and standard deviations for 3 or more spots on several different grains for each slide.

Olivines (Table 2) are chrysolites, $Fo_{80-81}$, and of similar composition from both samples. No significant differences in major or minor oxide content between samples is apparent. Orthopyroxenes (Table 3) are enstatites, $En_{77-79}$ $Wo_{04}$ $Fs_{17-19}$, with only minor variations in composition between the two sample areas. The western sample (Sample 7) contains orthopyroxenes slightly higher in FeO and $TiO_2$ and lower in MgO than Sample 25. Clinopyroxenes are diopsidic augite, $En_{41,53}$ $Wo_{36,48}$ $Fs_{11}$, with identical FeO contents (6.5 weight percent) for both samples. Significant compositional differences occur for $TiO_2$, $Al_2O_3$, MgO and CaO (Table 3); $Cr_2O_3$ and $Na_2O$ display minor variations between samples.

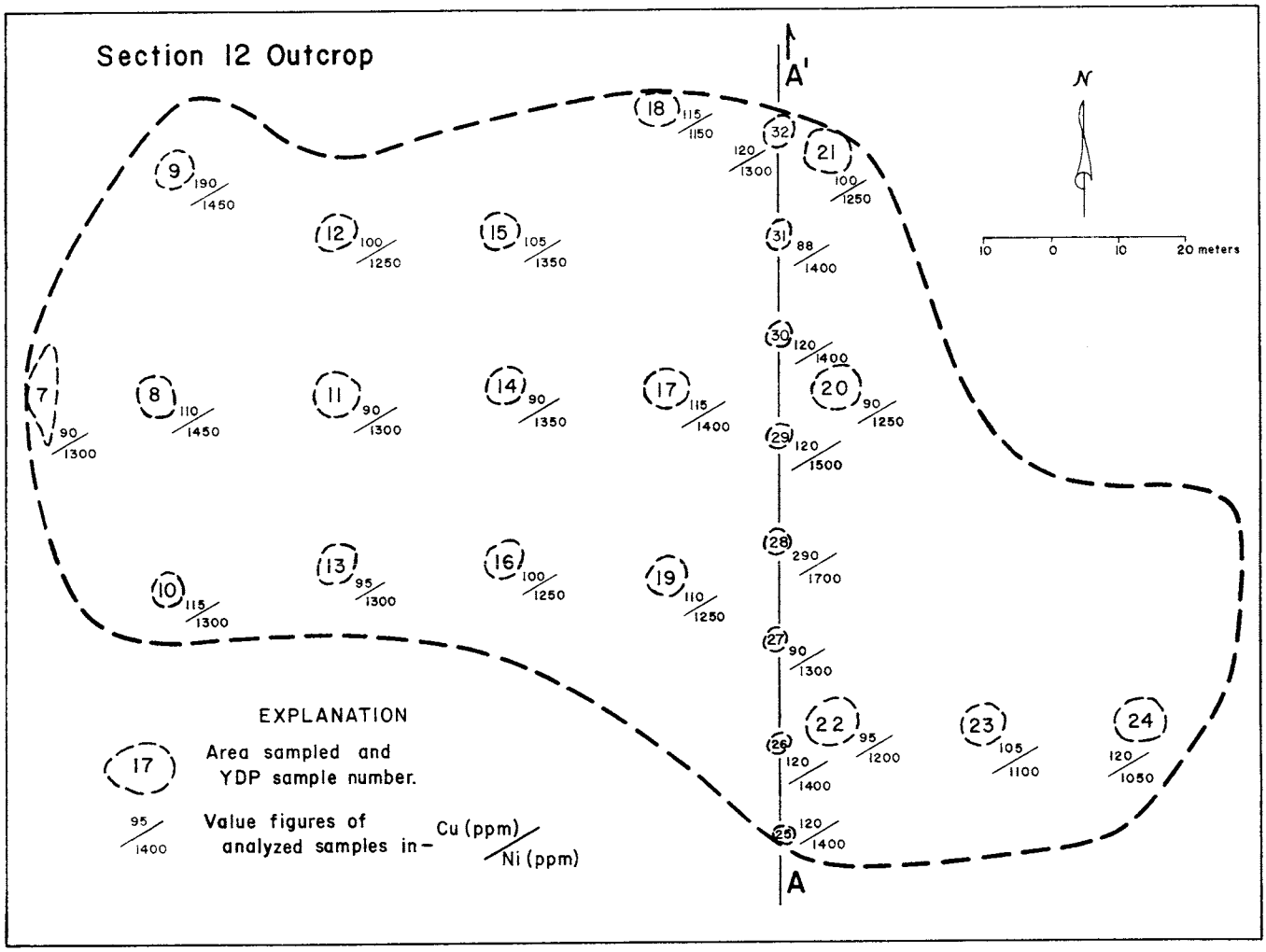


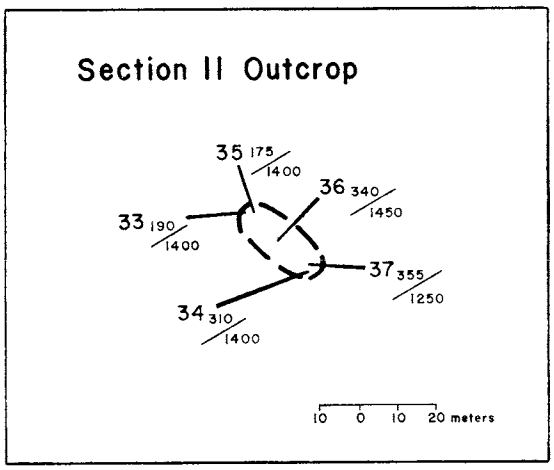


Figure 2. Location of analyzed samples. See Figure 3 for locations.

| Olivines | | |
|---|---|---|
| Oxide | YDP-7 | YDP-25 |
| $SiO_2$ | 38.88 ± .76 | 39.90 ± .41 |
| $TiO_2$ | 0.04 ± .04 | 0.01 ± .00 |
| $Al_2O_3$ | 0.05 ± .04 | 0.04 ± .02 |
| FeO* | 18.44 ± .93 | 17.81 ± .83 |
| $Cr_2O_3$ | 0.05 ± .04 | 0.03 ± .03 |
| MnO | 0.21 ± .08 | 0.20 ± .04 |
| NiO | 0.01 ± .02 | 0.00 ± .00 |
| MgO | 40.74 ± .79 | 42.21 ± .58 |
| CaO | 0.22 ± .09 | 0.26 ± .05 |
| $Na_2O$ | 0.01 ± .01 | 0.02 ± .02 |
| Total | 98.65 | 100.48 |
| Number of ions on the basis of 4 oxygens | | |
| Si | 1.010 | 1.010 |
| Al | 0.001 | 0.000 |
| Ti | 0.000 | 0.000 |
| ΣFe | 0.400 | 0.380 |
| Cr | 0.000 | 0.000 |
| Mg | 1.570 | 1.590 |
| Ni | 0.000 | 0.000 |
| Mn | 0.004 | 0.004 |
| Ca | 0.005 | 0.006 |
| Na | 0.000 | 0.000 |
| Total | 2.990 | 2.990 |
| * Total iron as FeO | | |

Table 2. Electron microprobe analyses of olivines from the Yellow Dog Peridotite expressed in weight percent.

Compositions of individual silicate minerals may be of partial use in determining parental magma type. The Yellow Dog Peridotite contains olivines with 80 to 81 mole-percent forsterite, a common composition for olivines found within many types of ultramafic rocks. Peridotitic komatiites typically contain more magnesian olivines, at $Fo_{89-94}$ (Nesbitt, 1971; Pyke et al., 1973; Arndt et al., 1977). These compositions are not limited to komatiitic rocks, however, as cumulate parts of several layered mafic-ultramafic intrusions of tholeiitic origin (e.g., Stillwater) locally contain high-magnesian ($>Fo_{90}$) olivines. Other elements do not appear to be diagnostic indicators. Olivine compositions are thus of little use in distinguishing komatiitic from tholeiitic magma suites.

Chemical data for komatiitic pyroxenes are scarce, but one genetic discriminating parameter may be the alumina content of clinopyroxenes. Microprobe studies of ultramafic lavas from Ontario (Pyke et al., 1973; Arndt et al., 1977) and western Australia (Nesbitt, 1971) indicate unusually high contents of $Al_2O_3$ in clinopyroxene, generally from 5 to over 8 weight percent. Such alumina contents normally imply high formational pressure (Green, 1967), a condition clearly

| Orthopyroxenes | | |
|---|---|---|
| Oxide | YDP-7 | YDP-25 |
| $SiO_2$ | 54.26 ± .59 | 55.24 ± .63 |
| $TiO_2$ | .57 ± .05 | 0.40 ± .10 |
| $Al_2O_3$ | 1.55 ± .25 | 1.84 ± .44 |
| FeO* | 12.17 ± .22 | 11.33 ± .48 |
| $Cr_2O_3$ | 0.32 ± .07 | 0.37 ± .08 |
| MnO | 0.25 ± .05 | 0.20 ± .04 |
| NiO | 0.11 ± .14 | 0.02 ± .03 |
| MgO | 27.84 ± .40 | 29.02 ± .31 |
| CaO | 1.99 ± .14 | 1.90 ± .17 |
| $Na_2O$ | 0.05 ± .04 | 0.04 ± .02 |
| Total | 99.11 | 100.36 |
| Number of ions on the basis of 6 oxygens | | |
| Si | 1.953 | 1.952 |
| Al | 0.065 | 0.076 |
| Ti | 0.015 | 0.010 |
| ΣFe | 0.366 | 0.334 |
| Cr | 0.008 | 0.010 |
| Mg | 1.493 | 1.528 |
| Ni | 0.003 | 0.000 |
| Mn | 0.007 | 0.005 |
| Ca | 0.076 | 0.071 |
| Na | 0.003 | 0.002 |
| Total | 3.989 | 3.988 |
| Clinopyroxenes | | |
| $SiO_2$ | 51.90 ± .55 | 51.71 ± .34 |
| $TiO_2$ | 0.45 ± .12 | 1.45 ± .10 |
| $Al_2O_3$ | 1.85 ± .37 | 2.71 ± .16 |
| FeO* | 6.53 ± .58 | 6.52 ± .17 |
| $Cr_2O_3$ | 0.92 ± .07 | 0.56 ± .05 |
| MnO | 0.13 ± .04 | 0.16 ± .03 |
| NiO | 0.09 ± .09 | 0.04 ± .07 |
| MgO | 18.49 ± .21 | 16.29 ± .13 |
| CaO | 17.57 ± .92 | 19.25 ± .39 |
| $Na_2O$ | 0.29 ± .02 | 0.43 ± .04 |
| Total | 98.22 | 99.12 |
| Number of ions on the basis of 6 oxygens | | |
| Si | 1.934 | 1.914 |
| Al | 0.080 | 0.117 |
| Ti | 0.012 | 0.040 |
| ΣFe | 0.203 | 0.201 |
| Cr | 0.027 | 0.016 |
| Mg | 1.025 | 0.898 |
| Ni | 0.002 | 0.001 |
| Mn | 0.004 | 0.004 |
| Ca | 0.700 | 0.763 |
| Na | 0.020 | 0.030 |
| Total | 4.007 | 3.984 |
| *Total iron as FeO | | |

Table 3. Electron microprobe analyses of pyroxenes from the Yellow Dog Peridotite expressed in weight percent.

precluded by the subaerial environment of these lavas. High alumina contents of komatiitic clinopyroxenes are probably the result of disequilibrium crystallization during rapid quenching of ultramafic liquids under surface conditions. Nevertheless, most other ultramafic rocks formed at low pressures have low $Al_2O_3$ in clinopyroxene (O'Hara, 1967), providing an empirical method to distinguish tholeiitic from komatiitic magmas crystallized under volcanic and subvolcanic conditions. Clinopyroxenes from the Yellow Dog Peridotite contain less than 3 weight percent alumina, and are compatible with bulk chemical data suggesting a tholeiitic rather than komatiitic affinity.

Differences in chemistry of clinopyroxenes for the two sample areas suggest somewhat different petrologic histories for the dikes. Modal proportions of olivine, orthopyroxene, and clinopyroxene are similar for both samples, and so variations in clinopyroxene composition reflect differences in crystal-melt equilibria during crystallization and/or slight differences in original bulk chemistry of magma between the two sites. The occurrence of primary calcic plagioclase ($An_{57-65}$) coexisting with spinel (and hornblende ?) suggests low pressure conditions along the univariant breakdown curve between the orthopyroxene - plagioclase - lherzolite facies and the spinel - lherzolite facies (O'Hara, 1967; Frost, 1976). This assemblage is stable within a much higher temperature-pressure range than local greenschist-facies rocks, thus reflecting original conditions of magma crystallization. Further work employing pyroxene geothermometers and geobarometers might define more closely the petrogenesis of the peridotite.

Nickel contents of the olivines and pyroxenes are contrary to predicted values based on experimentally determined distribution coefficients. In theory, olivines should contain much more nickel then coexisting pyroxenes. Recent detailed microprobe studies of similar Yellow Dog samples by W. J. Morris (1977) suggest that the olivines contain about 0.4 weight percent nickel, or roughly three times that of coexisting ortho- and clinopyroxenes. Since the values obtained in this investigation do not parallel the findings of W. J. Morris, we suspect an instrumental error in the anomalously low nickel values reported for our Yellow Dog olivines (Table 2).

## Opaque Mineralogy

Oxide and sulfide minerals typically make up 5 to 8 volume percent of the peridotite. Oxides are most abundant, and include ilmenite, magnetite, and minor to trace amounts of chromite and rutile. Ilmenite is the most common opaque mineral, occurring as rounded to irregular skeletal grains up to 2 millimeters in size. Most are interstitial to olivine and pyroxene grains, but some are poikilitically enclosed by large pyroxene crystals. Ilmenite grains are generally fractured and show textures suggesting partial resorption. Characteristically, they occur isolated without associated oxides or sulfides. The majority of ilmenite grains are optically homogeneous, but some display fine, 1- to 3-micron-wide, oriented [0001] lamellae of titanomagnetite and chromite (?). One presumably secondary inclusion of hematite was found along the margins of one ilmenite grain.

Magnetite occurs as both primary and secondary grains of variable size and shape. Primary magnetite is found as interstitial grains between silicates and as angular to rounded inclusions up to 0.5 millimeters in orthopyroxene. Secondary magnetite, formed by serpentinization of olivine and pyroxene, occurs as thin (5 to 10 microns) stringers between relict olivine crystals, and as isolated grains or clusters of grains surrounding or within altered pyroxenes. Some magnetite grains are complexly intergrown with sulfide minerals.

Chromite is a minor oxide phase found as polygonal to subrounded grains 0.1 millimeter in diameter, generally intergrown with relict olivine. Trace amounts of rutile occur as irregular isolated grains 0.1 millimeter in length; one crystal displays color zoning in transmitted light with yellowish, orange, and dark red-brown bands.

Sulfide minerals typically comprise 1 to 2 percent of the peridotite. Major sulfides are pyrrhotite, pentlandite, and chalcopyrite, with minor pyrite and cubanite and trace amounts of mackinawite. Traces of secondary marcasite, bornite and covellite are present in a few sections. Sulfide minerals occur as composite grains up to 3 millimeters in diameter; the majority are less than 0.1 millimeter in size. Most are irregularly shaped, fractured, and interstitial to silicates; some form 0.1 millimeter rounded inclusions or globules within pyroxene crystals. Sulfides show preferential association with magnetite, chiefly as chalcopyrite containing laths of magnetite. Less commonly, chalcopyrite occurs as myrmekitic intergrowths within certain magnetite grains. Cubanite and pentlandite generally occur with pyrrhotite or chalcopyrite. Complex intergrowths are common, mainly fine lamellae of chalcopyrite in cubanite and leaf-like blades of cubanite in pyrrhotite. Mackinawite occurs as small inclusions in cubanite.

Native nickel-iron alloy, probably awaruite, occurs as rare angular grains up to 15 microns in diameter both in areas of secondary silicates such as serpentine and talc, and as isolated inclusions in olivine or pyroxene crystals. It is most likely the result of a reducing environment generated during serpentinization, producing native metals from decomposed silicates and altered sulfides (Eckstrand, 1975; Botto and Morrison, 1976).

Textures of certain oxide and sulfide phases suggest liquid immiscibility with the crystallizing peridotite. Sulfide globules within pyroxenes are likely the result of sulfur saturation and subsequent sulfide liquid separation. Rounded inclusions of magnetite in pyroxenes and myrmekitic magnetite-chalcopyrite intergrowths suggest contemporaneous immiscibility of oxides and sulfides from the silicate melt.

## Trace Element Content

Selected trace element contents from the Sections 11 and 12 outcrops are given in Table 4. Some elements show significant increases in concentration relative to world averages for peridotite and other ultramafic rocks (Table 5). Most important are large anomalies for copper and sulfur, as well as zinc and possibly silver. Zinc contents are approximately double those for average ultramafic rock. Varying limits of detection shown on Table 5 preclude an accurate assessment of average silver values, but the presence of 0.2 ppm silver in four samples (Table 4) is clearly anomalous. Cobalt and nickel contents fall within typical ultramafic ranges; chromium is depleted by a factor of about two. Semiquantitative spectrographic analyses of 10 samples for 50 other elements failed, within detection limits, to identify any unusual metal concentrations.

Copper contents of 37 samples of the Yellow Dog Peridotite range from 90 to 350 ppm and average 150 ppm, compared to worldwide means of less than 50 ppm reported by various authors (Table 5). The copper is not evenly distributed between the two outcrops, with the smaller Section 11 outcrop considerably enriched relative to the Section 12 outcrop. The two outcrops average 270 and 120 ppm, respectively. Copper values are clearly anomalous in relation to most other ultramafic rocks.

Sulfur content is also distinctly higher in Yellow Dog Plains samples than in average ultramafic rock (Table 5). The most recent compilation of Wedepohl (1975) suggests 400 ppm (0.04 percent) as a mean sulfur value for ultramafic rock. Four Yellow Dog Peridotite samples yielded a range from 700 to 1740 ppm sulfur (0.070 to 0.174 weight percent), with an average of 1340 ppm (0.134 percent). Sulfur and copper contents may be used as effective discriminators of ore potential, utilizing the method of Cameron et al. (1971). The sulfur contents of over 1000 ultramafic rocks of the Canadian Shield were grouped by them into barren, minor ore, and ore categories, based on copper-nickel production figures. Barren ultramafics (N = 616 samples) display sulfur contents ranging from 0.011 to 0.327 weight percent, with a mean of 0.059 and standard deviation of 0.107. Minor ore samples (N = 91) vary from 0.029 to 0.879, with a mean and standard deviation of 0.177 and 0.559, respectively. Ultramafic rocks associated with 16

| Sample | Ag | Cu | Co | Cr | Ni | Zn |
|---|---|---|---|---|---|---|
| 1 | na | 160 | na | na | 1400 | na |
| 2 | na | 145 | na | na | 1400 | na |
| 3 | na | 335 | na | na | 1700 | na |
| 4 | na | 115 | na | na | 1200 | na |
| 5 | na | 340 | na | na | 1700 | na |
| 6 | na | 125 | na | na | 1300 | na |
| 7 | <.2 | 90 | 50 | 3000 | 1300 | <200 |
| 8 | <.2 | 110 | na | na | 1450 | na |
| 9 | <.2 | 190 | na | na | 1450 | na |
| 10 | <.2 | 115 | na | na | 1300 | na |
| 11 | <.2 | 90 | na | na | 1300 | na |
| 12 | <.2 | 100 | na | na | 1250 | na |
| 13 | <.2 | 95 | na | na | 1300 | na |
| 14 | <.2 | 90 | na | na | 1350 | na |
| 15 | <.2 | 105 | na | na | 1350 | na |
| 16 | <.2 | 100 | na | na | 1250 | na |
| 17 | <.2 | 115 | na | na | 1400 | na |
| 18 | <.2 | 115 | na | na | 1150 | na |
| 19 | <.2 | 110 | na | na | 1250 | na |
| 20 | <.2 | 90 | na | na | 1250 | na |
| 21 | <.2 | 100 | na | na | 1250 | na |
| 22 | <.2 | 95 | na | na | 1200 | na |
| 23 | <.2 | 105 | na | na | 1100 | na |
| 24 | .2 | 120 | na | na | 1050 | na |
| 25 | <.1 | 120 | 93 | 1300 | 1400 | 110 |
| 26 | <.1 | 120 | 95 | 1300 | 1400 | 120 |
| 27 | <.1 | 90 | 85 | 1300 | 1300 | 130 |
| 28 | <.1 | 290 | 93 | 1400 | 1700 | 110 |
| 29 | <.1 | 120 | 91 | 1300 | 1500 | 110 |
| 30 | <.1 | 120 | 86 | 1400 | 1400 | 120 |
| 31 | <.1 | 88 | 90 | 1400 | 1400 | 110 |
| 32 | <.1 | 120 | 86 | 1300 | 1300 | 130 |
| 33 | <.1 | 310 | 90 | 1300 | 1400 | 110 |
| 34 | <.1 | 190 | 95 | 1300 | 1400 | 120 |
| 35 | .2 | 175 | na | na | 1400 | na |
| 36 | .2 | 340 | na | na | 1450 | na |
| 37 | .2 | 355 | 50 | 2000 | 1250 | <200 |

Samples 1 through 6 from unspecified location on Section 12 outcrop, and 7 through 24 and 35 through 37 from locations shown on Figure 2. Analyzed by atomic absorption techniques by Rocky Mountain Geochemical Corp. except for Co, Cr, and Zn, which were spectrographic analyses by Skyline Labs Inc. Samples 25 through 34 are from locations shown on Figure 2, and analyses are by a semiquantitative spectrographic technique at U.S. Geological Survey analytical laboratories, Reston, Va.

na - not analyzed.

Table 4. Trace element content of the Yellow Dog Peridotite expressed in parts per million (ppm).

| | Ag | Cu | Co | Cr | Ni | Zn | S* |
|---|---|---|---|---|---|---|---|
| Turekian & Wedepohl (1961) | 0.06 | 10 | 150 | 1600 | 2000 | 50 | 300 |
| Vinogradov (1962) | 0.05 | 20 | 200 | 2000 | 2000 | 30 | 100 |
| Goles (1967) | -- | 30 | 110 | 2400 | 1500 | -- | -- |
| Fisher et al.(1969)** | -- | 41 | 101 | 3040 | 1581 | -- | -- |
| Wedepohl (1975) | 0.05 | 47 | 110 | 3090 | 1450 | 56 | 400 |
| Yellow Dog Peridotite | 0.2 | 150 | 87 | 1525 | 1350 | 117 | 1340 |
| Sample size(n) | (31) | (37) | (12) | (12) | (37) | (10) | (4) |

* Sulfur analyses provided by the Institute of Mineral Research, Michigan Technological University.

** Data recalculated specifically for 41 peridotites, excluding other ultramafic rock types.

-- = not given.

Table 5. Comparison of selected trace element contents for average ultramafic rock and the Yellow Peridotite expressed in parts per million (ppm).

major copper-nickel ore deposits (N = 372) contain from 0.112 to 1.92 percent sulfur, with a mean of 0.582 and standard deviation of 1.37. Although there is much scatter in the data, sulfur contents of the Yellow Dog Peridotite are most similar to the minor ore category, as defined by Cameron et al. (1971). Nickel and cobalt contents of major ore suites are not significantly enriched relative to typical ultramafic rocks (Cameron et al., 1971, p. 308), a pattern followed by Yellow Dog Plains samples (Table 5). Notably, copper was found to be the second most important discriminator of ore potential, after sulfur. Anomalously high copper and sulfur contents determined for Yellow Dog Plains samples suggest the possibility of economic copper-nickel mineralization at depth.

## PALEOMAGNETIC STUDIES

Seven hand specimens were collected from the two outcrops of the peridotite. Two cores from each sample were analyzed by Kenneth Books of the U.S. Geological Survey in the Reston magnetic laboratory. Measurements were made for susceptibility, direction and intensity of remanence. Susceptibility was converted to intensity of induced magnetism. Remanence data for natural remanent magnetization and for succeeding steps of alternating current cleaning up to 500 oersteds were analyzed by computer and a Fisher statistical analysis run for each step. The optimum cleaning step (least scatter of direction) appeared to be at 200 oersteds but even at that step the samples showed considerably more scatter than other lower Keweenawan rocks previously analyzed from the region. The virtual geomagnetic pole data are: latitude -58.68; longitude 142.62 east; delta m = 38.58; and delta p = 34.29. The "optimum" cleaned direction of magnetization for the peridotite is not significantly different statistically from some other lower Keweenawan directions of magnetization and is very similar to directions obtained for diabase dikes nearby (DuBois, 1962). The peridotite undoubtedly can be assigned a lower Keweenawan age.

The relatively large scatter and differing polarizations of the natural remanent magnetization obtained from different samples indicate secondary components of magnetization. These components may be at least partially responsible for the net north-seeking down magnetization in the peridotite and could produce the positive magnetic anomaly over the peridotite. Although probably small, another contributor to a positive anomaly over the peridotite might be the moderate intensity of the induced magnetization ($2.50 \times 10^{-3}$ emu/cm$^2$). This induced magnetization may be compared to the average intensity of remanent magnetization for the seven samples of $69.20 \times 10^{-3}$ emu/cm$^2$.

It is possible that secondary magnetite produced during serpentinization of part of the olivine has a normal remanent direction and is at least partly responsible for the scatter of pole positions and the positive magnetic anomaly.

## FIELD GEOPHYSICAL STUDIES

Although regional aeromagnetic data (Case and Gair, 1965) and regional gravity data (Klasner, 1977) are already available, further geophysical studies were conducted to determine more precisely the size and location of the peridotite bodies. These studies consisted of detailed surveys near the peridotite outcrops in Sections 11 and 12, T50N, R29W, plus more widely spaced surveys located along an east-west belt about 20 kilometers long and at a greater distance from the outcrops. Gravity (Figure 3), ground magnetic (Figure 4) and VLF-EM (Figure 5) techniques were used in the detailed survey area. Ground magnetic and VLF-EM profiles were measured along selected lines outside the detailed area (see Figures 1 and 6).

The combined use of all three geophysical techniques greatly restricts the spectrum of possible geologic bodies responsible for the measured anomalies and allows a closer approach to a unique solution than would be possible with any single technique. Complications of

interpretation arise, however, from several factors. Most important are: 1) the complexities of the magnetic field caused by the interaction of the induced field and the irregularly oriented natural remanent field; 2) the possible variations in density of the peridotite due to variable degrees of serpentinization; 3) imprecise knowledge of the densities of all rock types in the area; 4) variations in thickness of Pleistocene drift; and 5) the imprecise understanding of the composition of the buried conductive bodies that produced a measurable VLF-EM response.

In spite of these difficulties, much useful information has been obtained on the geologic nature of the area, and geophysical models were prepared that seem consistent with the observed geological and geophysical data.

## Field Procedures and Data Reduction

### Gravity

Figure 3 shows the gravity coverage in the detailed study area and the location of two regional profiles. In the detailed study area, nine gravity profiles spaced 400 meters apart were measured in a north-south direction, roughly perpendicular to the trend of the aeromagnetic anomaly. Station spacing on the profiles was 152 meters. The two regional profiles extend across the southernmost aeromagnetic anomaly as well as the northern anomaly.

Gravity values were measured with a LaCoste and Romberg model G land gravimeter. Drift checks, taken at bench mark 1422 every three hours or less, had less than 0.1 milligal drift per hour. The gravity readings were tied to the Marquette gravity base.

Most elevations were determined by leveling between U.S. Geological Survey benchmarks. North of the base line (see Figure 3), surveys closed within 5 centimeters; south of the baseline, where swamps made surveying difficult, elevation surveys closed within 18 centimeters or better. A few elevations shown on Figure 3 were determined by altimeter with an estimated accuracy based on repeated readings of 1.6 meters or less. All distances were measured with a steel tape and have an estimated accuracy of 98% or greater.

The gravity data were reduced using the 1967 international gravity formula, a 427-meter above sea level datum, and a Bouguer density of 1.7 g/cm$^3$. The 1.7 g/cm$^3$ value is the density of the sand and silt that covers the bedrock and was determined from a density profile measured over a small topographic feature in the sand plains.

### Ground Magnetics

Figure 4 shows the ground magnetic coverage in the detailed study area as well as several profiles that were extended southward into Sections 13 and 14. North of the base line, seventeen profiles were measured; south of the base line ten profiles were measured. Station spacing along the profiles was 30.3 meters. North of the base line, station spacing was measured with a steel tape and south of the base line distances were determined by pace.

Figure 6 shows the regional ground magnetic coverage. Outside of the detailed study area, twenty profiles were measured with spacing between profiles from 800 to 1,200 meters. Five profiles from Figure 4 are included in Figure 6 to maintain continuity of coverage. Station spacing for the regional profiles was 30.3 meters and was determined by pace.

All readings were taken with a Geometrix model G816 proton precession magnetometer in the backpack mode. Base checks for magnetic drift were made at bench mark 1422 every three hours or less. Data were discarded if the magnetic drift exceeded 20 gammas per hour.

Inasmuch as all data were tied to a common base, this base served as a reference for the magnitude of the total magnetic field in this area. It was assigned a value of 59,780 gammas, based on the average of 25 readings which had a total range of 60 gammas (59,766 to 59,826 gammas).

### VLF-EM

VLF-EM coverage in the detailed study area consisted of 16 lines, shown on Figure 5. All readings were taken with a Geonics EM-16 unit facing north. The station spacing along the profiles was 30 meters, determined by pace. Transmitter locations used in the survey were NLK, Seattle, Washington (18.6 kHz) and NAA, Cutler, Maine (17.8 kHz).

The location of two lines of regional VLF-EM coverage is shown on Figure 1. Line 1 is the southern extension of the westernmost line in the detailed study area. It extends across the southernmost aeromagnetic anomaly. Line 3, located 9 kilometers west of the detailed study area, crosses both the northern and southern aeromagnetic anomalies. Station spacing on both lines was 30 meters, determined by pace.

To make the VLF-EM data easier to interpret and to smooth noisy data, all of the profiles, including both the in-phase and quadrature components, were filtered by a method outlined by Fraser (1969). The filter is a difference operator and low-pass filter that smooths the data and transforms zero crossovers into peaks and troughs, depending on the direction of the crossover. These filtered data are then contoured into positive and negative anomalies as shown on Figure 5.

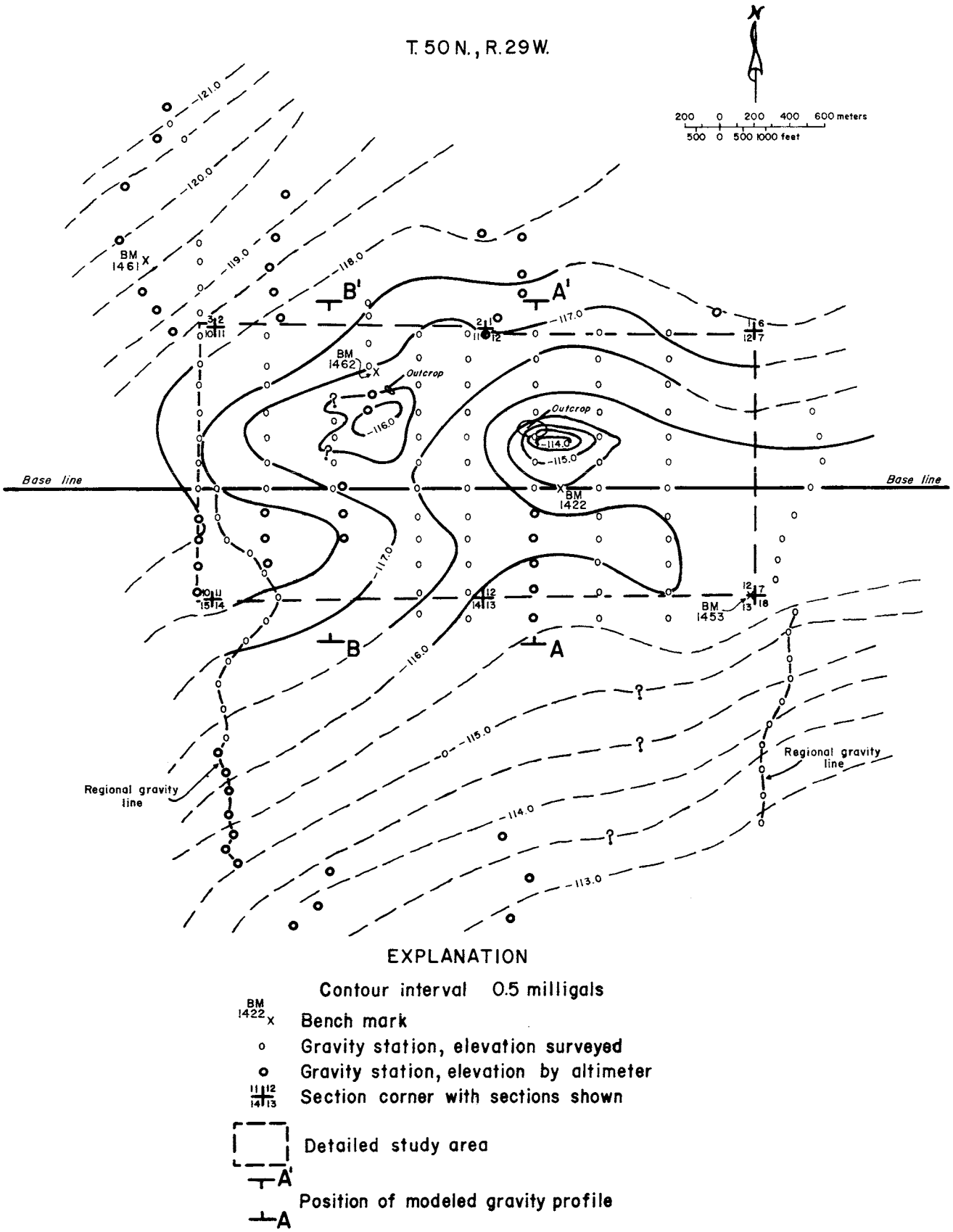


Figure 3. Complete Bouguer gravity anomaly.

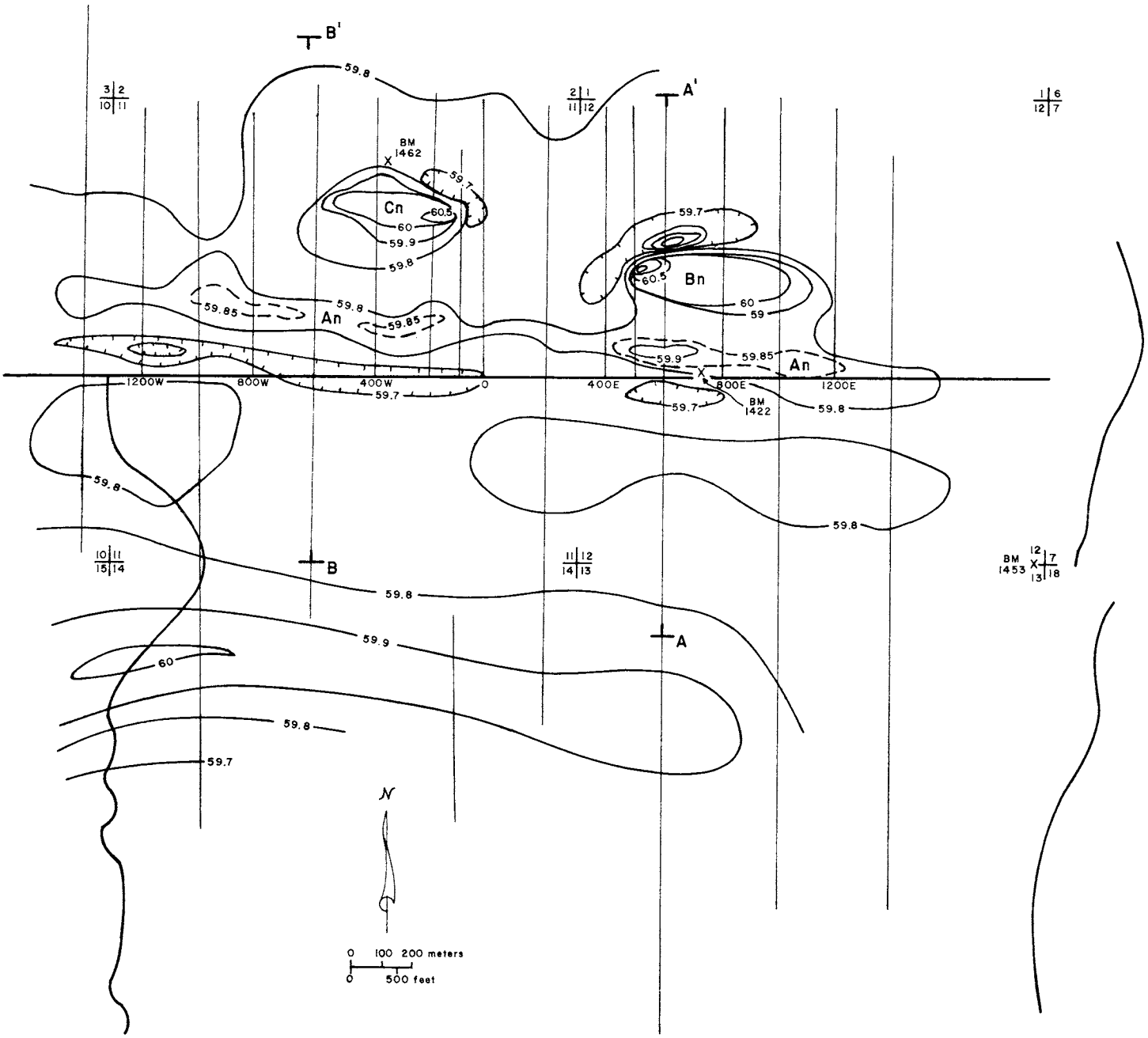


## EXPLANATION

Contour interval in thousands of gammas, interval spacing 500 gammas above 60.0 and 100 gammas below 60.0

Extra contour for detail

A' — A — Location of modelled profile

Location of ground magnetic profiles

Field surveys by: A. Grosz, P. Geraci, R. Lilienthal, D. Snider, 1976

An, Bn, Cn Anomaly designation

Figure 4. Ground magnetics of detailed study area.

## Interpretation of Geophysical Data

Figure 5 shows that both positive and negative VLF-EM anomalies are present in the detailed study area. Positive in-phase anomalies, which ideally have a positive peak flanked by nearly symmetrical negative shoulders, generally indicate the presence of anomalous conductivity. Negative in-phase anomalies ideally have a pronounced trough with nearly symmetrical positive shoulders. Negative VLF-EM anomalies may be caused when: A) a resistive body is located in a field of more conductive material, such as a resistive dike outcropping in a swamp or area of conductive clay (Ronka, Patterson, written communication), or B) a dike with a high magnetic permeability and a low degree of conductivity causes a response in the VLF-EM receiver coils due to the natural magnetic field overriding the electromagnetically induced field (Grant and West, 1965).

It appears from this study that the negative in-phase VLF-EM anomalies are caused by conditions similar to the second situation (B) outlined above. Two of the negative anomalies (Bn and Cn) occur over the peridotite outcrops in areas of thick dry sand. And all of the negative VLF-EM anomalies have associated positive magnetic anomalies.

The positive VLF-EM anomalies (Figure 5), on the other hand, do not have associated positive magnetic anomalies. In fact there seems to be little, if any, associated magnetic expression.

It is significant that, with the exception of anomalies Cp and the northwest extension of Bp, all VLF-EM anomalies, both positive and negative, have associated positive residual gravity anomalies suggesting that the bodies which cause the electromagnetic anomalies are denser than the enclosing country rock. A cluster of mafic dikes, denser than the enclosing country rock as shown in Figure 7, could cause this unique combination of geophysical anomalies. The nature of these dikes is discussed in the following paragraphs.

In order to interpret the gravity data, it is necessary to separate the Bouguer gravity anomaly map (Figure 3) into regional and residual components. This was done graphically by the cross profile method, and Figure 8 shows the different components into which the Bouguer anomaly was separated. $R_1$ represents the regional gravity gradient. No map has been prepared for this surface. $R_2$ is a regional surface, possibly caused by basement faulting or by variations in thickness of Pleistocene cover or both, as discussed below. $R_3$ is the observed Bouguer gravity anomaly. Residual gravity maps were prepared by subtracting $R_1$ from $R_2$ to form gravity residual-1, as shown in Figure 9, and $R_2$ from $R_3$ to form gravity residual-2, as shown in Figure 10. Theoretical two-dimensional gravity models (Talwani et al., 1959) were constructed along profiles AA' and BB' (Figures 11a and 11b) to try to explain the residual gravity-2 anomalies.

Preliminary geologic reports (Trow, 1978 a,b,c) for three holes drilled recently in the Baraga Basin near the area of study provide valuable data for construction of the gravity models. Approximate location of the three holes is shown on Figure 1. Holes DL-1 and DL-7 are located near the north edge of the Baraga Basin, whereas DL-3 is located in the south half of the basin. For the purpose of the gravity modeling, the most important points to be considered from the drilling are: a) depth of overburden varies from zero to over 260 feet, b) gamma-ray density logs indicate that the bulk density of middle Precambrian rocks ranges from 2.80 to 2.85, and c) in the north half of this part of the Baraga Basin, depth to basement is greater than 545 meters and in the south half it is greater than 1,000 meters.

Rock density measurements from chip samples of Yellow Dog Peridotite and rock density data from published work provide additional information for construction of the models. Density measurements on two separate samples of the peridotite indicate that the density may vary from at least 2.83 $gm/cm^3$ to 2.95 $gm/cm^3$. This range is much lower than the average density of fresh peridotite (3.23 $gm/cm^3$) as reported in the Handbook of Physical Constants (Clark, 1966) and is probably related to the degree of serpentinization of the peridotite. Recent mapping in Archean terrain south of the Baraga Basin shows that basement rocks are predominantly syenite with 10 to 25 percent mafic gneiss. North of the basin, drill hole DL-7 encountered granodiorite in the basement, but this area has not been mapped in sufficient detail to determine how much, if any, mafic gneiss is intermixed with the granodiorite. According to Clark (1966), the average density for syenite is 2.76 $gm/cm^3$ and for granodiorite it is 2.72 $gm/cm^3$. Considering a density of 2.92 to 3.15 $gm/cm^3$ for mafic gneiss (Klasner and Cannon, 1974; Klasner et al., 1978), basement rocks south of Baraga Basin could have an average density as high as 2.85 $gm/cm^3$ and the rocks north of the basin could have an average density of 2.72 $gm/cm^3$ or greater, depending on the percentage of mafic gneiss intermixed with granodiorite. At any rate, Precambrian W basement rocks appear to have about the same density as the overlying Precambrian X rocks.

In summary, then, the major factors to be considered in construction of the gravity models and interpretation of the gravity residual maps (Figures 9 and 10) are as follows:

A) Density ranges permissible for modeling are 1.7 $gm/cm^3$ for Pleistocene drift, about 2.80 to 2.85 $gm/cm^3$ for Precambrian X rocks, about 2.75 to 2.85 $gm/cm^3$ for Precambrian W basement rocks, and 2.83 to 2.95 for peridotite.

B) The density contrast between drift and underlying bedrock is about -1.10 gm/cm$^3$. This large contrast in density makes variations in drift thickness an important factor in modeling. For example, a change in thickness of drift from 30.3 meters to 45.5 meters creates a 1.3+ milligal anomaly, which is an amount nearly as large as the variation in residual gravity shown on Figure 9.

C) Depths to Archean basement must be greater than the 545-meter and 1,000-meter drill hole depths in the north and south parts of the basin, respectively.

Because of the small density contrast between basement and Precambrian X rocks, and our imprecise knowledge of variations in drift thickness, no attempt was made to model the depth and configuration of the Baraga Basin. It is possible, however, that the south-sloping gradient in the gravity residual-1 (Figure 9) is caused by a down-to-the-south fault in the basement as suggested in previously constructed preliminary models (Klasner et al., 1977), or it may reflect the presence of a deeply buried mafic body of rock beneath the Baraga Basin.

The east-west trending, positive gravity anomaly (gravity residual-2) shown in Figure 10 can be explained, for the most part, by three east-west trending dikes as shown on Figures 11a and 11b. The combined gravitational effect of the dikes explains the 1,200-meter width of the anomaly. The position of the dikes is controlled by outcrops at Bn and Cn, the location of positive magnetic anomalies and negative electromagnetic anomalies (An), and the location of positive electromagnetic anomalies (Ap and Bp). Depth to the top of the dikes and dike width are not extremely critical parameters in the model. Therefore, these factors in the model should be considered rough approximations only.

Although the gravity residual-2 can be roughly explained by the dikes, it was necessary to include a layer of Pleistocene drift of varying thickness to create a closer match between observed and calculated gravity. This layer of very low density material, however, lowered the average amplitude of calculated gravity to a value well below that of the observed gravity residual-2. To counteract this, a large pod of dense mafic rock buried at ten to fifteen thousand feet below the ground surface is included in the model. Inasmuch as the mineralogy and chemical composition of the peridotite suggests that it formed by differentiation from a basaltic magma, the presence of such a mafic body at depth has geologic merit. However, more information is necessary to either confirm or refute this; therefore, this part of the model is intended primarily to illustrate that the gravity data permit the interpretation that a large mafic rock mass exists at depth. Other models could be constructed to explain the observed gravity data.

The important point to note in these two models (Figures 11a and 11b) is that the gravity data suggest excess mass beneath the magnetic and electromagnetic anomalies. The only alternate explanation that might be employed to explain such a unique combination of gravity, magnetic, and electromagnetic anomalies is abrupt high-frequency variations in drift thickness with accompanying magnetic and electromagnetic effects. In particular, this rationale might be used to explain anomalies Ap and Bp. Although they have positive electromagnetic anomalies, they do not have accompanying magnetic anomalies. It is possible that ridges of graphitic slate stick up into the overlying drift and cause both the electromagnetic and gravity expression.

On the Bouguer gravity anomaly map of the Baraga-Dead River basins area (Klasner, 1977), a large, low amplitude, positive gravity anomaly is centered about two miles northeast of the detailed study area. This anomaly, which is at least one mile in diameter and about two milligals in amplitude, may represent a buried mafic body of rock that was once the magma chamber from which the Yellow Dog Peridotite differentiated. The anomaly appears geophysically continuous with the positive gravity anomalies over the detailed study area and may represent the northeastward continuation of the deeply buried mafic body postulated in the two-dimensional gravity models.

## Interpretation of Individual VLF-EM Anomalies

The map of VLF-EM anomalies (Figure 5) shows four positive anomalies, Ap, Bp, Cp and Dp. Anomaly Ap, which has the highest amplitude, is probably offset by a small northwest-trending fault. Gravity model AA' (Figures 9, 11a) shows that it can be caused by a 30-meter-thick dike. Because it does not have an associated ground magnetic anomaly, the causative material may be something other than peridotite, and the anomalous conductivity indicated by the positive VLF-EM anomaly suggests that it may contain sulfide mineralization. Estimated depth to the top of the conductive body from VLF-EM data is 37 meters.

VLF-EM anomaly Bp is probably a compound anomaly. The high-intensity part of the anomaly (20 arbitrary filtered units) may be due, in part, to clay and electrolyte solutions in the underlying swamp. However, the EM profile along 1000W has a negative in-phase/quadrature relationship which may indicate a subsurface conductor other than the swamp. This possibility is supported by gravity model BB' which shows a 76-meter-thick dike at Bp near line 600W. There is only a slight magnetic anomaly over the dike, indicating small amounts of magnetite, but the positive EM anomaly indicates the possibility of sulfide mineralization. VLF-EM data on line 1000W suggests that the conductive body is 45 meters below the surface.

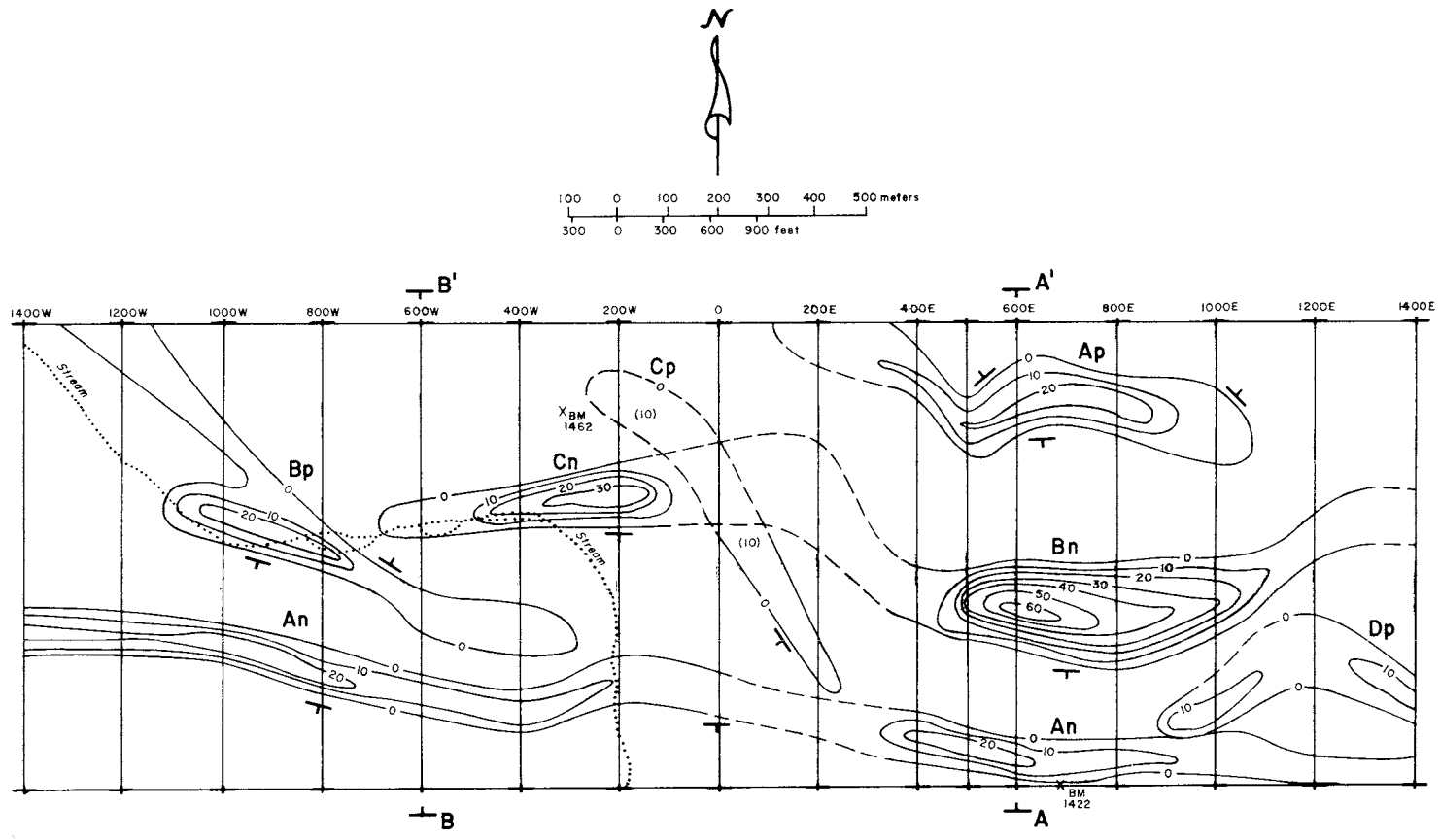


## EXPLANATION

Ap — Positive in-phase anomalies.

An — Negative in-phase anomalies.

1200W — Indicates line no. and position.

Contour Intervals: 10 Arbitrary filtered units. Dashed lines are uncertain contours.

Apparent dip direction.

A' A — Position of modeled profile.

### Transmitter Stations

Lines 1400W — 200E
Cutler, Me. 17.8 kHz

Lines 400E — 1400E
Seattle, Wash. 18.6 kHz

Figure 5. Filtered VLF-EM anomalies.

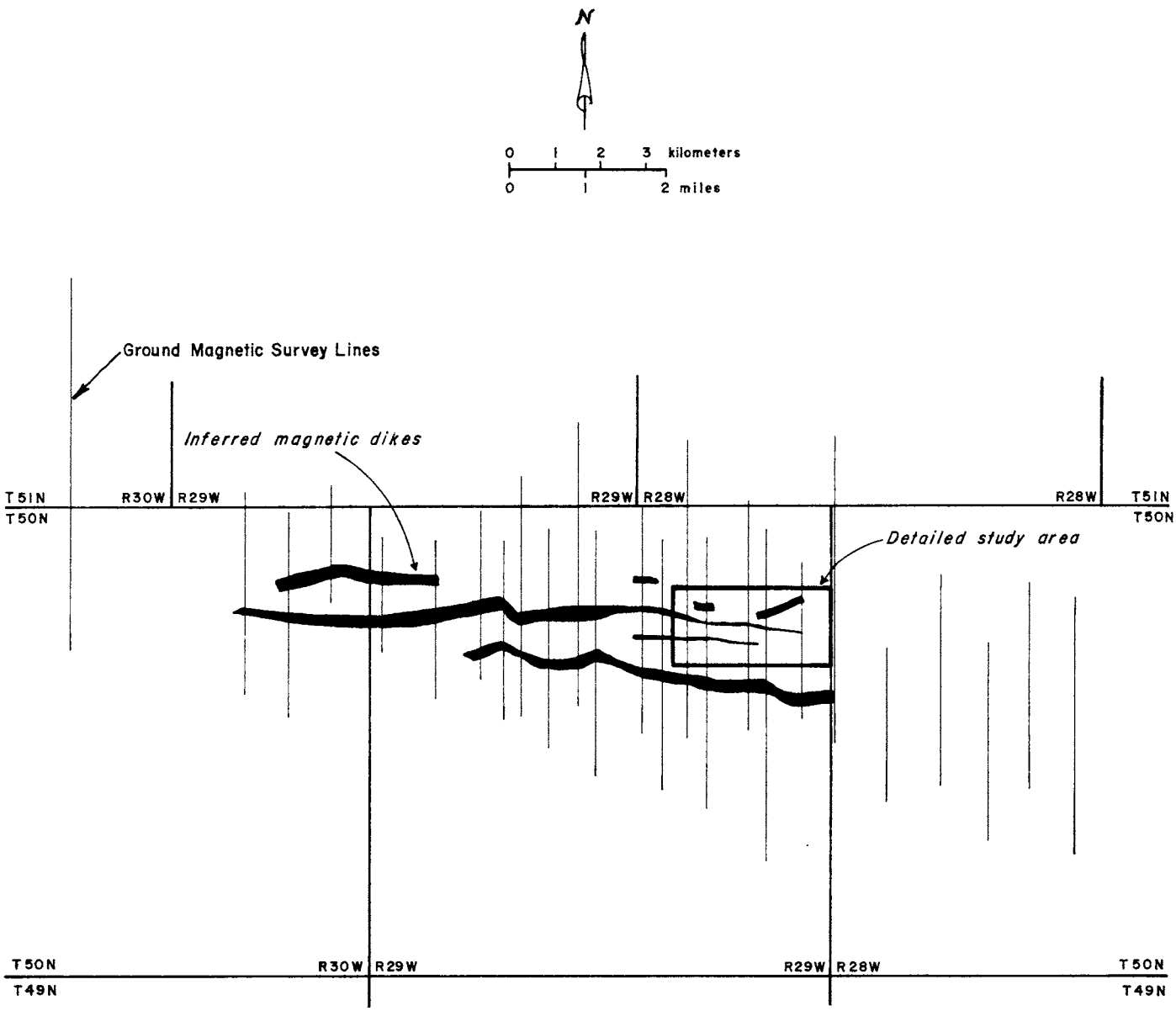


Figure 6. Dikes inferred from ground magnetics.

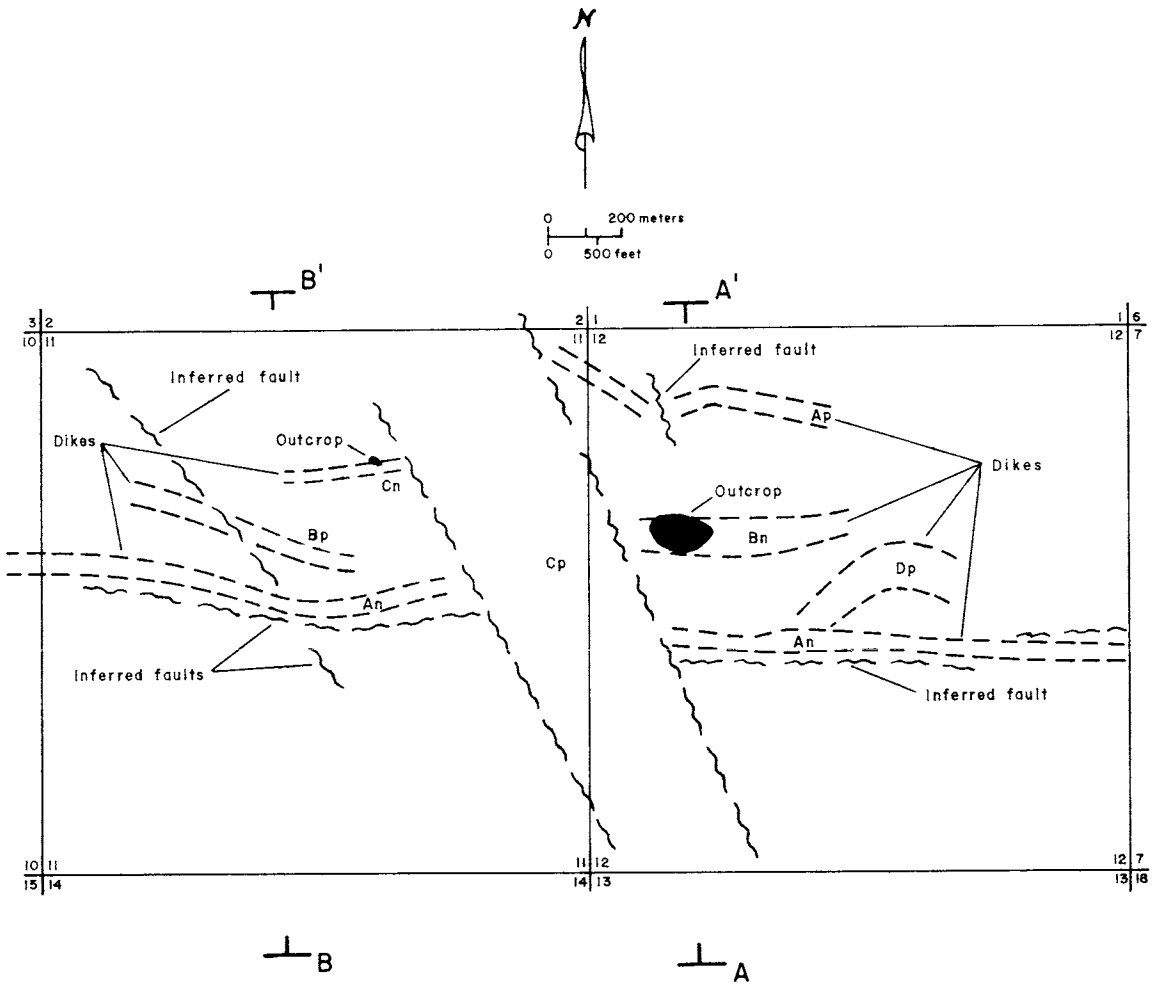


## EXPLANATION

A' — Location of modelled gravity profile — A

An, Ap — Letter designating location of geophysical anomaly, with subcript n meaning negative VLF-EM in-phase anomaly and subcript p meaning positive VLF-EM in-phase anomaly.

Figure 7. Geology of the detailed study area inferred from geophysical surveys.

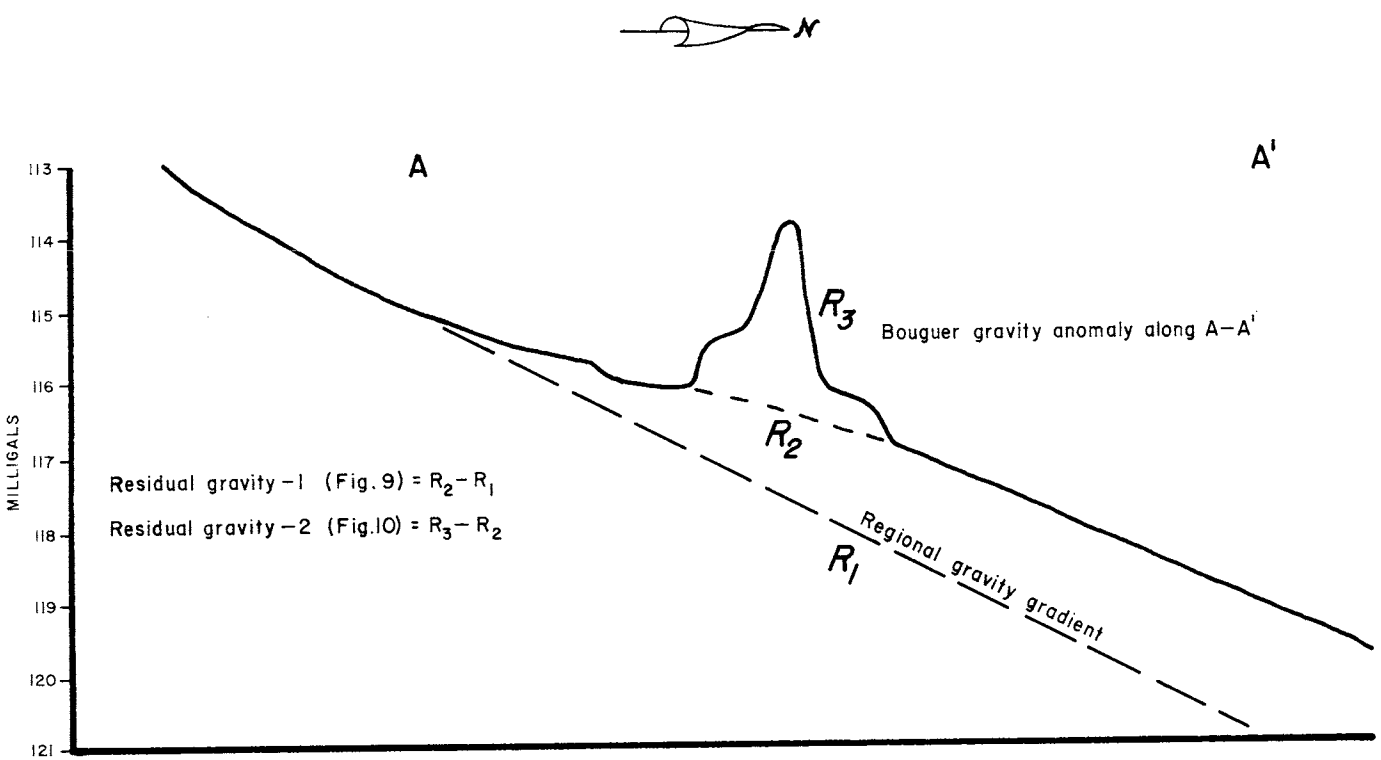


Figure 8. Gravity profile along A - A', showing how residual gravity anomalies were determined.

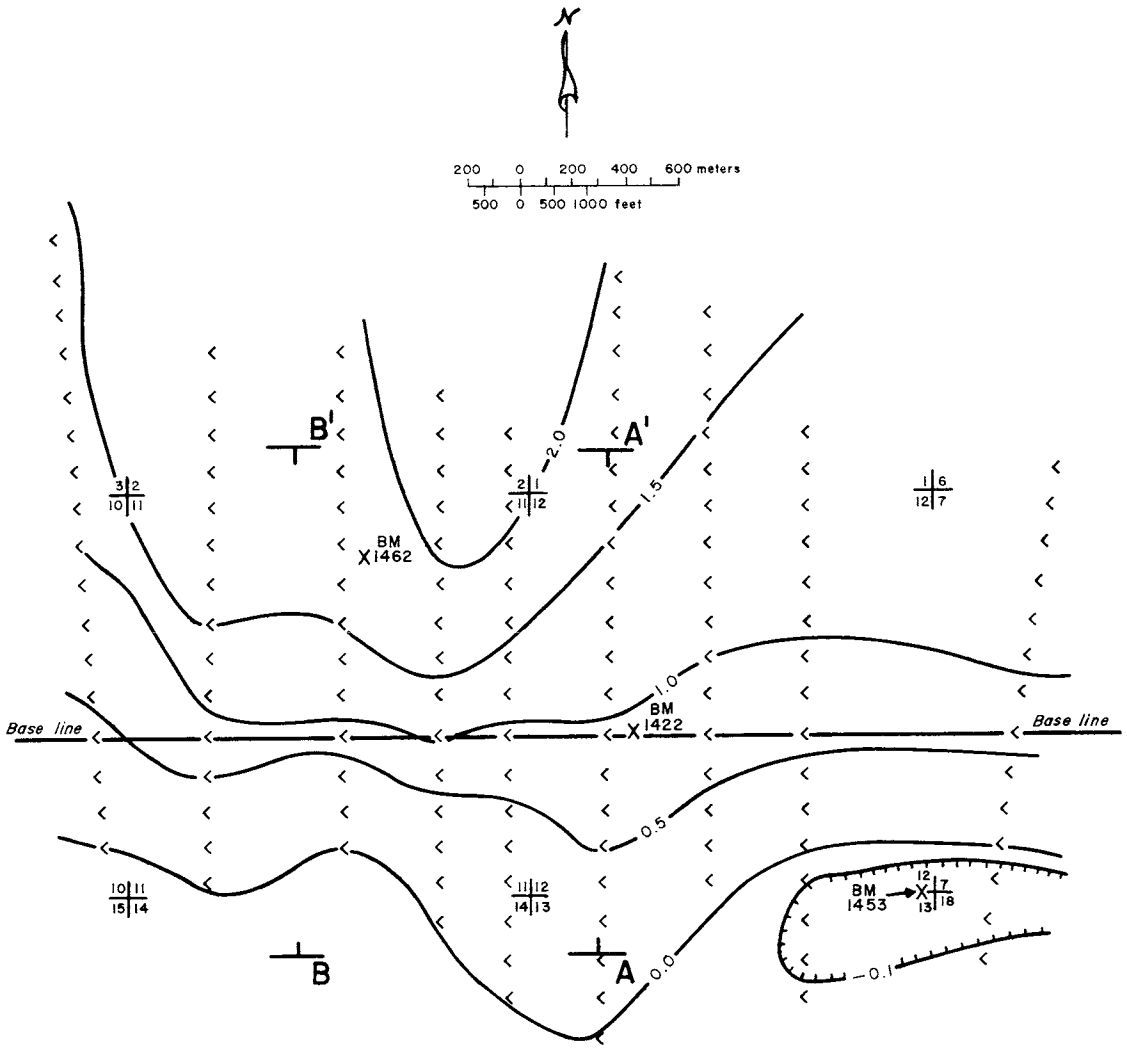


**EXPLANATION**

**Contour interval: 0.5 milligals**

**Location of control from graphic analysis**

**Section corner with sections shown**

**Bench mark**

**Position of modeled gravity profile**

Figure 9. Gravity residual - 1, anomaly caused by deep body.

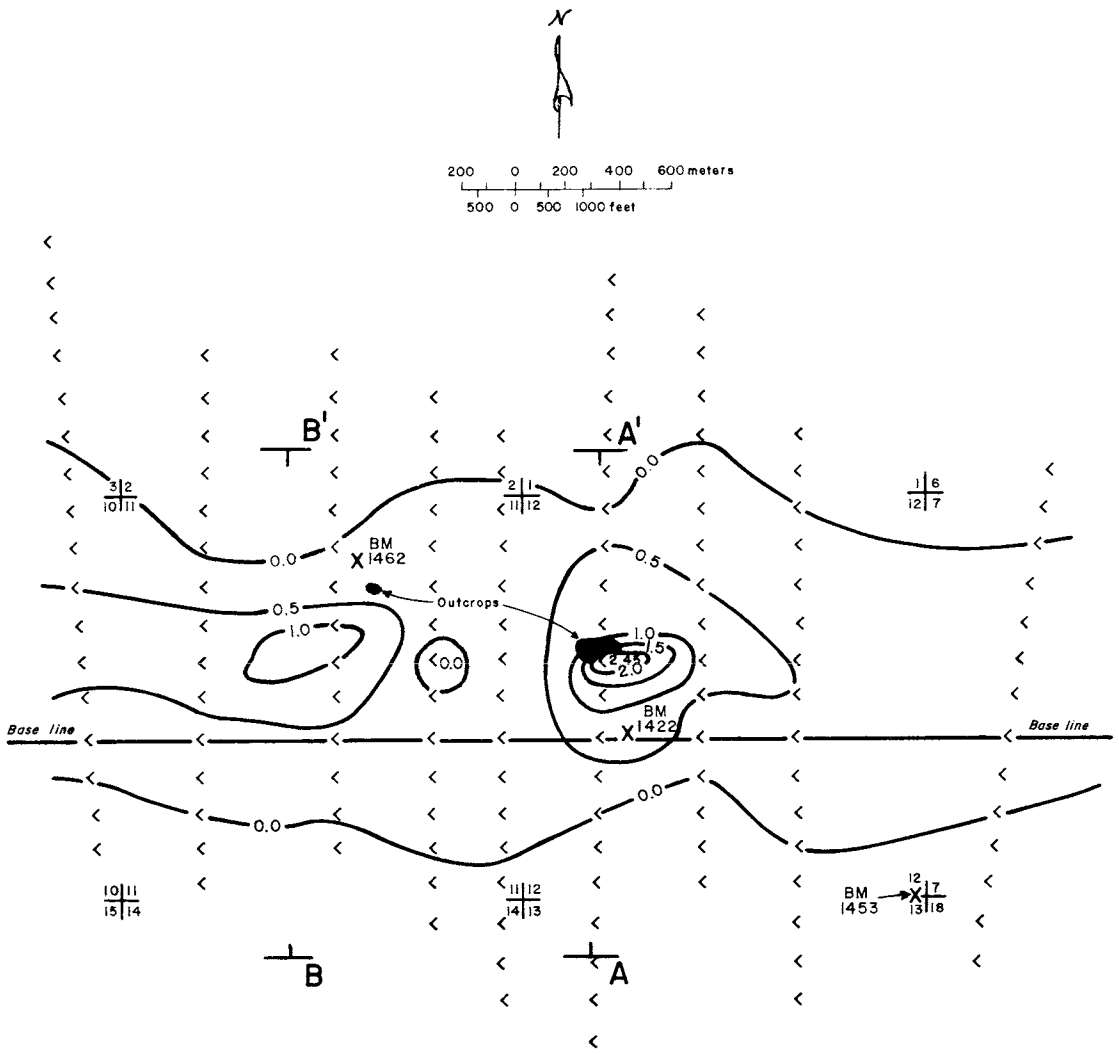


## EXPLANATION

**Contour interval: 0.5 milligals**

**Location of control from graphic analysis**

**Section corner with sections shown**

**Bench mark**

**Position of modeled gravity profile**

Figure 10. Gravity residual - 2, anomaly caused by near-surface dikes.

Both the positive VLF-EM anomaly Cp and the northwest extension of Bp trend north-northwest at a large angle to other electromagnetic anomalies in the area. The VLF-EM anomalies may be caused by electrolytic solutions or metallic mineralization in the shear zone of faults. Their rather low intensity may be due to the fact that the strike of the causative feature is at a high angle to the survey direction and not perpendicular to the nearly north-south transmitted electromagnetic field direction, so that a less-than-maximum coupling of the conductor with the transmitted field was achieved.

VLF-EM anomaly Dp has a maximum intensity of slightly more than ten arbitrary units. It falls within an area of a slight positive gravity anomaly but has no magnetic expression. VLF-EM data indicate that the top of the causative body is about 30 meters below the surface. The nature of the causative body is not known.

Three negative anomalies occur in the filtered VLF-EM data, An, Bn, and Cn, shown on Figure 5. Anomaly An is continuous in an east-west direction for about 2,800 meters, the total extent of the detailed study area. Locally it has an amplitude of 20 units, which may be due to the causative body being very near the surface. The anomaly is very weak in the area of the northwest-trending fault zone (lines 00 and 200E). Anomaly An is coincident with a magnetic anomaly (compare Figure 5 with Figure 4 and see also Figures 11a and 11b). Gravity data suggest that the causative body is a vertical dike about 30 to 45 meters thick. As with all of the negative VLF-EM anomalies, the combined VLF-EM and magnetic data indicate that the causative bodies have high magnetic permeability, probably caused by magnetite.

Negative VLF-EM anomaly Bn has the highest absolute intensity of any of the EM anomalies. It overlies a peridotite outcrop but is much larger in area than the outcrop. It is coincident with an intense (1700 gammas above background) ground magnetic anomaly. Gravity model AA' (Figure 11a) shows that the causative feature may be a vertical dike about 90 meters thick. All geophysical data indicate that the dike ends abruptly near the west edge of the outcrop. It is probably truncated by a northwest-trending fault.

VLF-EM anomaly Cn is also associated with a peridotite outcrop. The anomaly trends east-west and is much narrower and smaller in amplitude than Bn. Gravity model BB' (Figure 11b) indicates that the anomaly may be caused by a 30-meter thick vertical dike. This dike is also abruptly terminated at the northwest-trending fault zone.

A summary of data and interpretation of the anomalies shown on Figure 5 is listed on Table 6.

## Regional Survey

Regional geophysical coverage outside of the area of the detailed survey was designed to accomplish two objectives: 1) to test the continuity of the inferred dikes in an east-west direction, and 2) to examine the VLF-EM response in the area of the aeromagnetic anomalies at three locations.

The continuity of the magnetic anomalies away from the area of the peridotite outcrops is illustrated on Figure 6. The anomalies can be traced for about 20 kilometers and are approximately coincident with the aeromagnetic anomalies of Case and Gair (1965), thus suggesting that a swarm of dikes, at least some of which are peridotite, underlie the area. The southernmost inferred dike on Figure 6, which corresponds to the southern aeromagnetic anomaly, is at least 8 kilometers long. Other dikes do not appear to be as long, although the discontinuous nature of some of the anomalies may be due to post-Keweenawan faulting, to variations in magnetic mineral content, or to changes in the remanent magnetism along the strike of the dikes.

Figure 12 shows two of the regional profiles measured to obtain more information on the nature of the aeromagnetic anomalies. Profile 1 extends south from the base line near the western edge of the detailed study area for 2,400 meters and crosses the southern aeromagnetic anomaly. There is no VLF-EM response over the aeromagnetic anomaly, but ground magnetic measurements confirm the presence of the aeromagnetic anomaly. We interpret these data to indicate that a magnetic dike is present but is too deep to be detected by VLF-EM measurements. The absence of a gravity anomaly in the area indicates that the dike is either very thin or has a density close to that of the surrounding rocks.

Regional Profile 2 is not shown on Figure 12 but is incorporated into the gravity and magnetic maps (Figures 3 and 4). The profile is similar to Profile 1 and our interpretation of the anomalies is the same as for Profile 1.

Regional Profile 3 (Figure 12) starts at a road intersection in the NE1/4 SW1/4 Section 11, T50N, R30W and extends for 2,424 meters to the north, across the two aeromagnetic anomalies. Ground magnetic measurements on this profile confirmed the presence of the two aeromagnetic anomalies and also show anomalous readings near the south end of the profile. In all, five VLF-EM Anomalies (A through E on Figure 12) warrant discussion:

Anomaly A - This anomaly has a corresponding ground magnetic anomaly and a negative in-phase VLF-EM anomaly. The in-phase/quadrature relationship suggests that the filtered EM anomaly may not be real. Further electromagnetic studies are needed to test for the presence of an anomalous body.

| Anomaly | VLF-EM Sign | Ground Magnetics | Gravity | Causative Feature | Orientation and Extent | Estimated Depth to Body | Remarks |
|---|---|---|---|---|---|---|---|
| An | - | + 59,900 gammas | positive anomaly, modelled 61 m thick | nearly vertical dike | generally N 75° W 2.8 km long | - | probable magnetite mineralization |
| Bn | - | + 61,500 gammas | positive anomaly, modelled 120 m thick | nearly vertical dike | E-W about 800 m long | outcrops | see petrographic analyses |
| Cn | - | + 60,000 gammas, complex body suggested | positive anomaly, modelled 30 m thick | nearly vertical dike | N 80° E 600 m long | outcrops | see petrographic analyses |
| Ap | + | no apparent expression | positive anomaly, modelled 30 m thick | nearly vertical dike | N 80° W 1 km long | 37 m, VLF-EM | possible sulfide mineralization |
| Bp | + | only minor magnetic expression | positive anomaly, modelled on line 600 W 76 m thick | compound swamp, dike, and fault | N 45° W 900 m long | 45 m on line 1000 W, VLF-EM | compound anomaly possible sulfide mineralization |
| Cp | + | no apparent expression | zero to negative anomaly | fault zone | N 25° W about 800 m long | - | geophysics does not indicate sulfide mineralization |
| Dp | + | no apparent expression | slight positive anomaly, not modelled | unknown | irregular generally E-W about 400 m long | - | causative body not known but VLF-EM suggests conductivity |

Table 6. Summary of data and interpretations of anomalies. See Figure 5 for locations.

Anomaly B - The filtered VLF-EM data indicate the presence of an underlying relatively flat, wide (545 meters) conductive body. Ground magnetics show a slight positive anomaly near the south edge of the body, but otherwise the magnetic profile is featureless in this area. The VLF-EM data indicate that the causative body is about 30 meters below the surface. The anomaly may be caused by graphitic slate.

Anomalies C, D, and E - These three VLF-EM anomalies are negative and lie near the edges of the ground magnetic and aeromagnetic anomalies. The cause of the anomalies is not known but could be either resistive dikes or a rock with high magnetic permeability.

## GEOCHEMICAL SURVEY

Because the Yellow Dog Peridotite is much richer than the surrounding rocks in certain elements such as copper, nickel, cobalt, zinc, chromium, and magnesium, geochemical analysis of soils in areas of the positive aeromagnetic anomalies might give additional confirmation of the presence of buried peridotite. Near the peridotite outcrops and in most of Yellow Dog Plains, the Pleistocene drift cover is relatively thick and is mostly porous stratified sand and gravel. The probability that a geochemical anomaly from buried bedrock would be present in soil developed on the drift is slight and such areas were not tested. The westernmost extension of the magnetically anomalous area has thinner drift cover and the drift is mostly till. We determined that chances were good to detect anomalous bedrock compositions by soil analyses in that area.

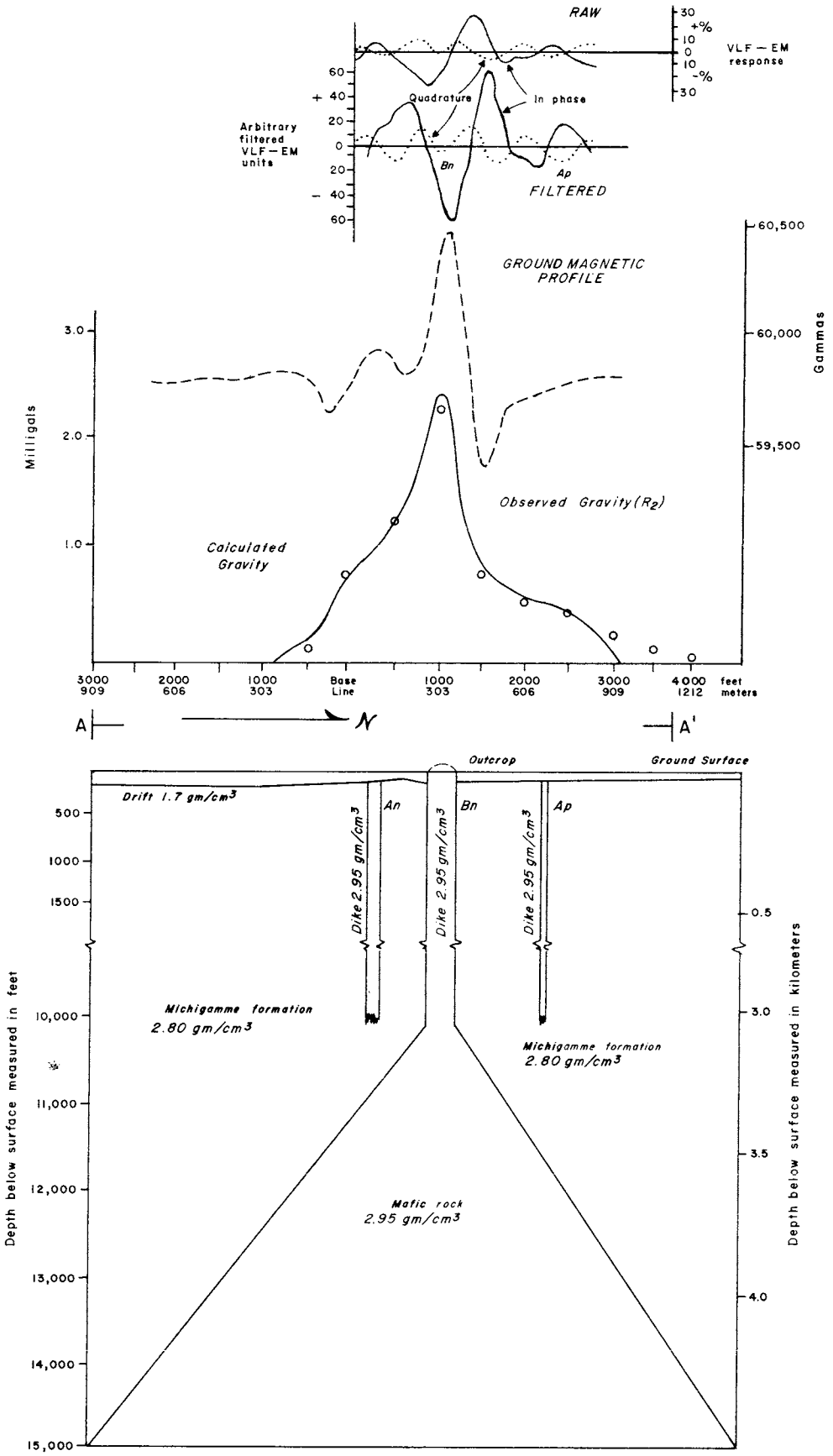


Figure 11 a. Composite geophysical profiles and geologic model for cross section A - A'.

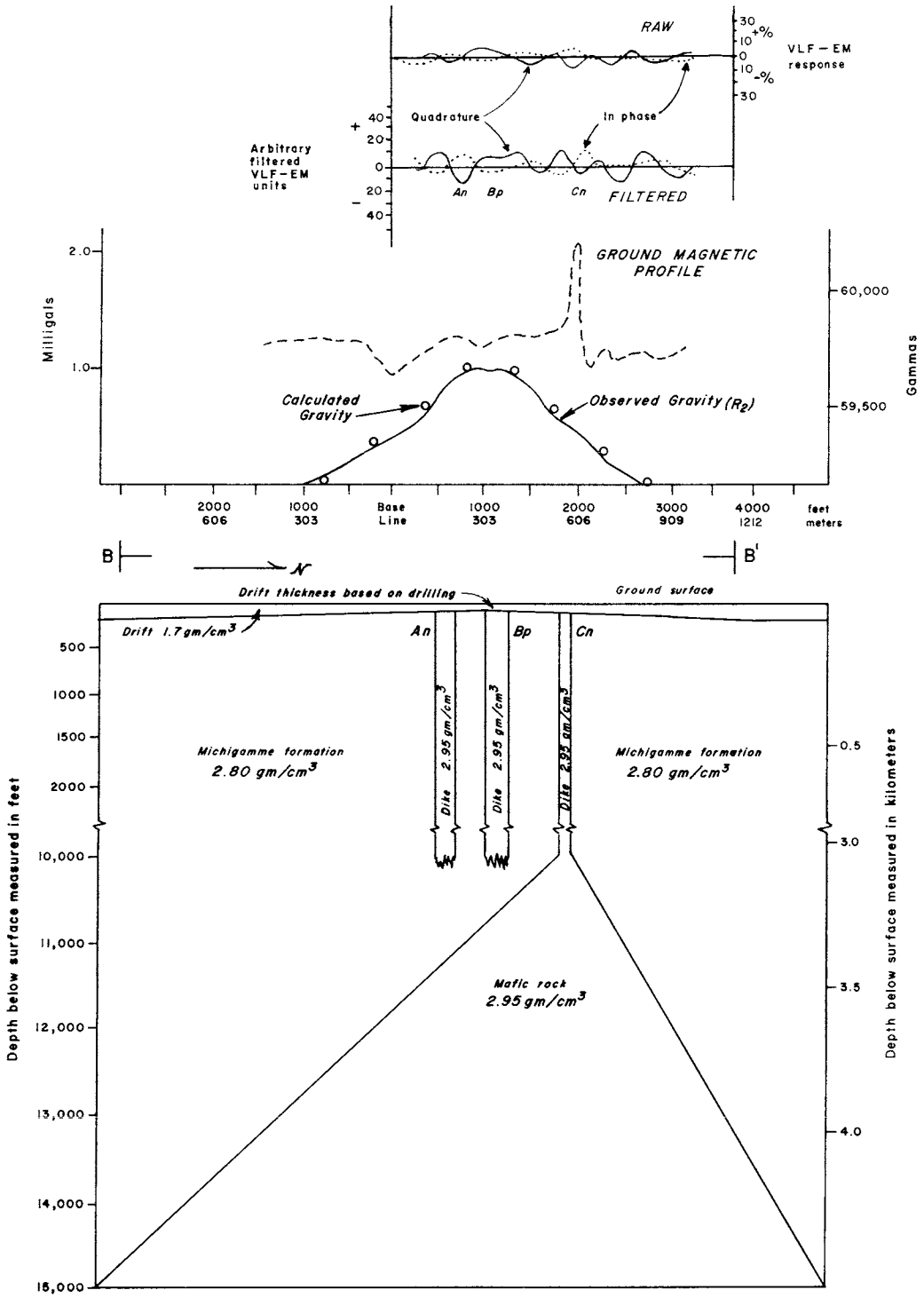


Figure 11 b. Composite geophysical profiles and geologic model for cross section B - B'.

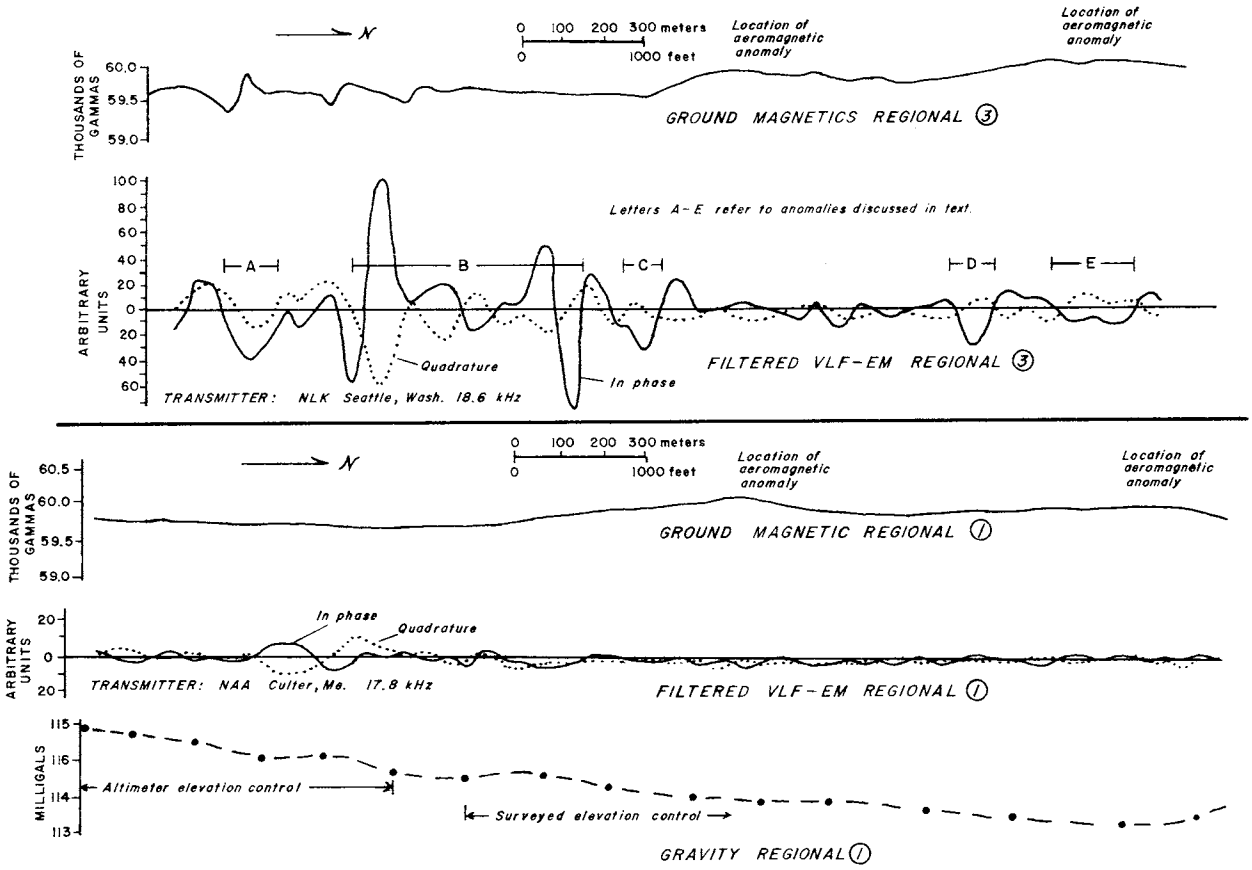


Figure 12. Composite geophysical profiles along regional lines 1 and 3.

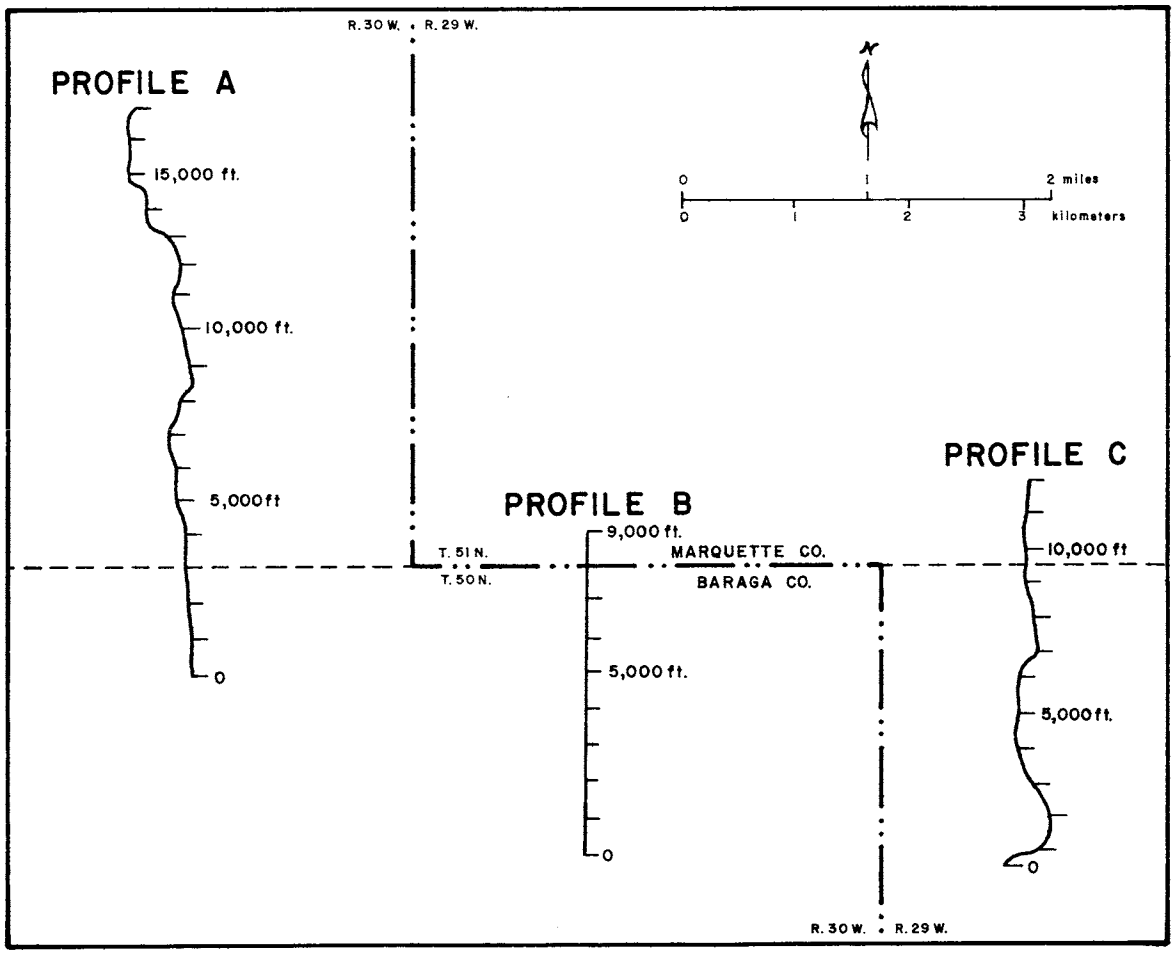


Figure 13. Location of geochemical soil profiles.

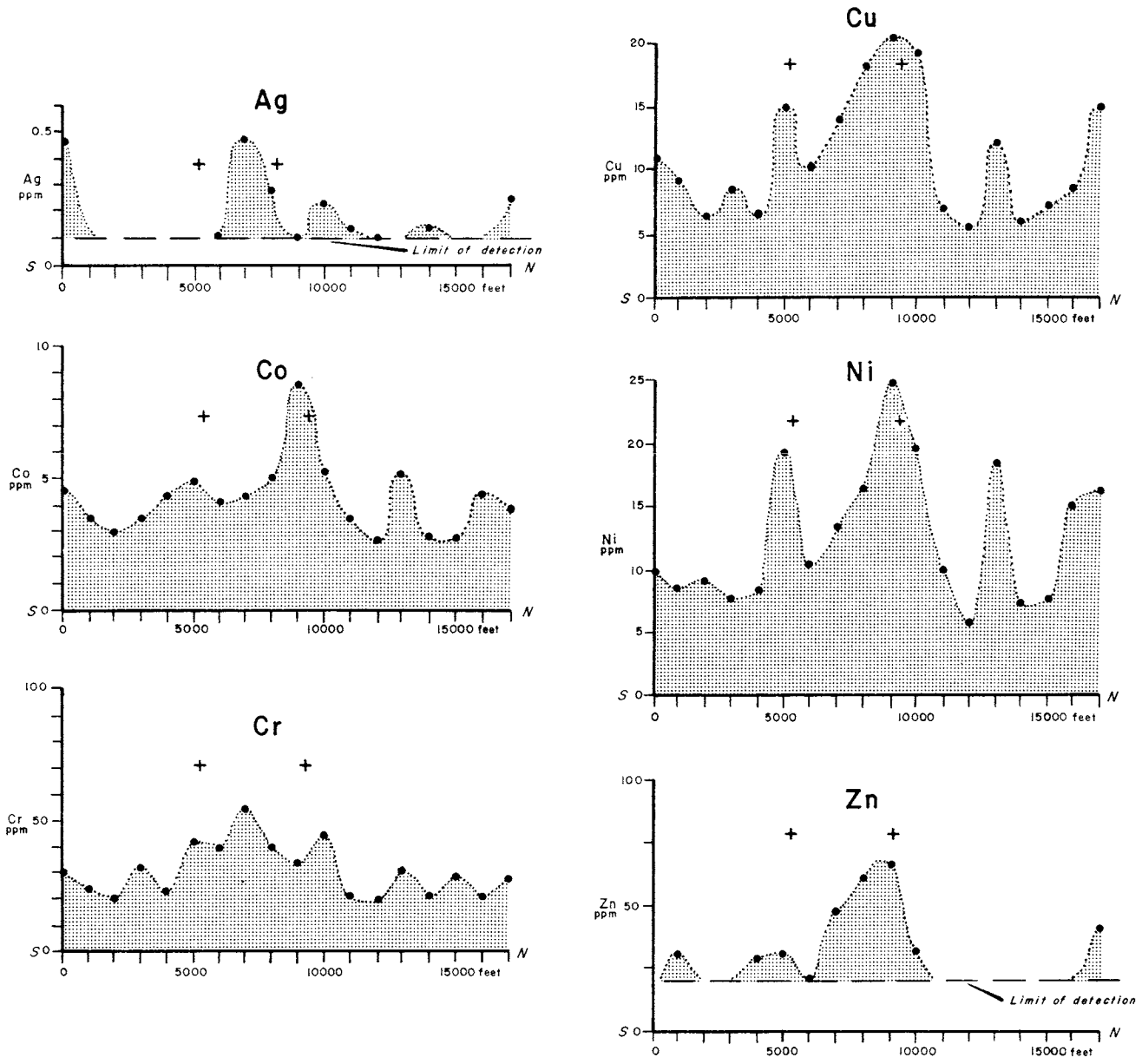


Figure 14. Geochemical profiles in soil along profile A.

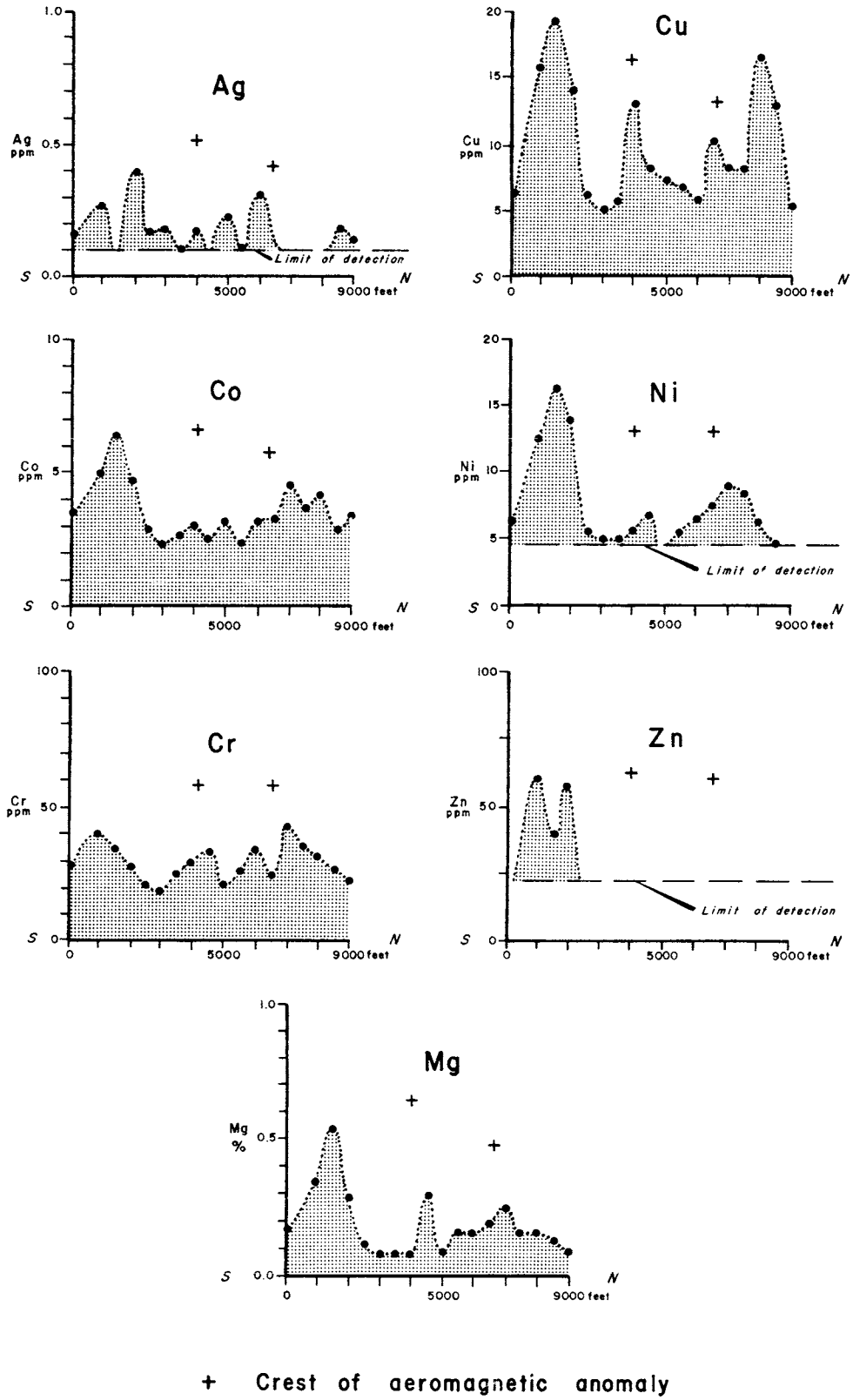


Figure 15. Geochemical profiles in soil along profile B.

Samples were collected along north-south traverses, shown in Figure 13, that crossed both the northern and southern aeromagnetic anomalies. Samples were taken roughly 40 centimeters below the surface, generally below the organic-rich upper soil horizons. Most of the material sampled was reddish brown sandy soil. In the laboratory the samples were sieved and the minus 80-mesh fraction was analyzed for 65 elements by a semi-quantitative spectrometric technique at the U.S. Geological Survey analytical laboratories in Reston, Virginia.

The results show that weak geochemical anomalies occur at or near the magnetic anomalies on two of the three profiles (Profiles A and B, Figure 13). The third profile (C) had no anomalies but is mostly on thick sand deposits of the Yellow Dog Plains through which effective geochemical communication between soil and bedrock is unlikely. Figures 14 and 15 show the content of elements along Profiles A and B. On Profile A, a broad anomalous area with higher than average values for cobalt, copper, nickel, and zinc coincides with the northernmost aeromagnetic anomaly. A narrower, weaker anomaly in these elements is suggested near the southernmost aeromagnetic anomaly. Silver and chromium also appear to be slightly anomalous in the areas of the magnetic anomalies. Likewise, two separate anomalous areas occur on Profile B. A weak cobalt-copper-nickel anomaly is near the northernmost aeromagnetic anomaly. A more pronounced anomaly in silver, cobalt, copper, nickel, and zinc is about 0.4 kilometer south of the southernmost magnetic anomaly. There is a suggestion of higher-than-average chromium with both anomalies but the relationship is weak. The southernmost anomaly on B also has higher-than-average magnesium content, but the three remaining anomalies do not have high magnesium values. This may indicate that the anomalies are caused mostly by elements such as copper, cobalt, nickel, and zinc being released from sulfide minerals during weathering, whereas magnesium and chromium, although abundant in the peridotite or mafic rocks, are held in less readily-weathered silicate or oxide minerals.

Earlier work by the U.S. Geological Survey in the region immediately west of the area of this study disclosed weak soil anomalies that are clearly related to weakly anomalous zones in the Michigamme Formation. There, the anomalies in both bedrock and soil are expressed by all or some of the elements that are anomalous on profiles A and B, plus lead and molybdenum. The soil anomalies A and B do not have anomalous lead and molybdenum values and chromium appears more consistently high there than in anomalies related to the Michigamme Formation. The suite of anomalous elements in profiles A and B mirrors the element distribution of peridotite more closely than the element distribution in the Michigamme Formation.

## SUMMARY AND CONCLUSIONS

Peridotite of early Keweenawan age is exposed at two outcrops in Sections 11 and 12, T50N, R29W, in an area generally mantled with Pleistocene outwash and till. Geophysical studies indicate that the peridotite is an east-west elongate body at least 1.5 kilometers long. Gravity, ground magnetic, and VLF-EM surveys have disclosed several other anomalies nearby with the same trend as the peridotite. Some of these anomalies extend at least 15 kilometers west and 5 kilometers east of the peridotite outcrops and are coincident with a 20-kilometer-long aeromagnetically anomalous zone consisting of two parallel positive anomalies about 1 kilometer apart.

Eight to 12 kilometers west of the outcrops, geochemical soil anomalies of several elements, abundant in the peridotite, are coincident with the aeromagnetic positive anomalies and may indicate that peridotite extends that far west. Therefore, with decreasing degrees of certainty, peridotite and related rocks can be inferred in a belt from as little as 1.5 to as much as 20 kilometers long.

The chemical composition and texture of the peridotite from the outcrops lead the authors to believe that it is a differentiate from a less mafic magma rather than a komatiite-like ultramafic rock. Thus, it seems likely that a larger body of mafic rock from which the peridotite has formed by fractional crystallization and differentiation lies buried somewhere in the region. A broad, low frequency and low amplitude gravity anomaly near the peridotite outcrops may be caused by such a body at depth.

Highly differentiated mafic rocks can be hosts for a variety of ore deposits, including copper, nickel, chromium and precious metals. The peridotite in the two outcrops contains an average of 150 ppm copper and some samples contain as much as 355 ppm. Sulfur contents range from 0.07 to 0.174 percent. The rock is considerably richer in both copper and sulfur than average peridotite, and in that respect resembles ore-bearing peridotites in other parts of the Canadian Shield. Positive EM anomalies such as Ap and Bp in areas of positive gravity anomalies may be caused by zones of sulfide concentrations in peridotite or mafic rocks, and need further study to determine the nature of the conductive body. Should the anomalies be shown to be caused by sulfide mineralization, the 20-kilometer-long magnetically anomalous zone would be a well-defined exploration target for extensions of that mineralization.

The Yellow Dog Peridotite is the only lower Keweenawan peridotite known in northern Michigan. Its tectonic significance is not yet known. Paleomagnetic data indicate that it is approximately the same age as the Duluth

Complex in Minnesota. Prior to middle Keweenawan rifting it probably was much closer to the Duluth Complex than it is now. Perhaps there is a genetic relationship between the Yellow Dog and Duluth rocks. If the two are comagmatic, the Yellow Dog Peridotite may be a favorable host rock for copper-nickel mineralization similar to that found in parts of the Duluth Complex.

---

## REFERENCES


Arndt, N. T., A. J. Naldrett, and D. R. Pyke, 1977, KOMATIITIC AND IRON-RICH THOLEIITE LAVAS OF MUNRO TOWNSHIP, NORTHEAST ONTARIO, Journal of Petrology, v. 18, p. 319-369.

Bence, A. E., and A. L. Albee, 1968, EMPIRICAL CORRECTION FACTORS FOR THE ELECTRON MICROANALYSIS OF SILICATES AND OXIDES Journal of Geology, v. 76, p. 382-403.

Botto, R. I., and G. H. Morrison, 1976, JOSEPHINITE: A UNIQUE NICKEL-IRON, American Journal of Science, v. 276, p. 241-274.

Cameron, E. M., G. Siddeley, and C. C. Durham, 1971, DISTRIBUTION OF ORE ELEMENTS IN ROCKS FOR EVALUATING ORE POTENTIAL: NICKEL, COPPER, COBALT, AND SULPHUR IN ULTRAMAFIC ROCKS OF THE CANADIAN SHIELD, The Canadian Institute of Mining & Metallurgy Special Volume 11, p. 298-313.

Cannon, W. F., 1973, THE PENOKEAN OROGENY IN NORTHERN MICHIGAN, The Geological Association of Canada Special Paper 12, p. 251-271.

___, and J. S. Klasner, 1977, GEOLOGIC MAP AND GEOPHYSICAL INTERPRETATION OF THE WITCH LAKE QUADRANGLE, MICHIGAN, United States Geological Survey Miscellaneous Geologic Investigations Map I-987.

Case, J. E., and J. E. Gair, 1965, AEROMAGNETIC MAP OF PARTS OF MARQUETTE, DICKINSON, BARAGA, ALGER AND SCHOOLCRAFT COUNTIES, MICHIGAN AND ITS GEOLOGIC INTERPRETATION, United States Geological Survey Geophysical Investigations Map GP-467.

Clark, S. P., Jr., 1966, HANDBOOK OF PHYSICAL CONSTANTS, Geological Society of America, Memoir 97, 587 p.

Coleman, R. G., and T. E. Keith, 1971, A CHEMICAL STUDY OF SERPENTINIZATION - BURRO MOUNTAIN, CALIFORNIA, Journal of Petrology, v. 12, p. 311-328.

Dubois, P. M., 1962, PALEOMAGNETISM AND CORRELATION OF KEWEENAWAN ROCKS, Geological Survey of Canada Bulletin 71, 75p.

Eckstrand, O. R., 1975 THE DUMONT SERPENTINITE: A MODEL FOR THE CONTROL OF NICKELIFEROUS OPAQUE MINERAL ASSEMBLAGES BY ALTERATION REACTIONS IN ULTRAMAFIC ROCKS, Economic Geology, v. 70, p. 183-201

Fisher, D. E., O. Joensuu, and K. Bostrom, ELEMENTAL ABUNDANCES IN ULTRAMAFIC ROCK AND THEIR RELATION TO THE UPPER MANTLE, Journal of Geophysical Research, v. 74, p. 3865-3873.

Fraser, D. C., 1969, CONTOURING VLF-EM DATA, Geophysics, v. 34, p. 958-967.

Frost, B. R., 1976, LIMITS TO THE ASSEMBLAGE FORSTERITE-ANORTHITE AS INFERRED FROM PERIDOTITE HORNFELSES, ICICLE CREEK, WASHINGTON, American Mineralogist, v. 61, p. 732-750.

Goles, G. G., 1967, TRACE ELEMENTS IN ULTRAMAFIC ROCKS, In; ULTRAMAFIC AND RELATED ROCKS, Wyllie, P. J., (Ed.) John Wiley and Sons, New York: New York, p. 352-362.

Grant, F. S., and F. G. West, 1965, INTERPRETATION THEORY IN APPLIED GEOPHYSICS, McGraw-Hill Book Co., New York: New York.

Green, D. H., 1967, HIGH-TEMPERATURE PERIDODITE INTRUSIONS, In; ULTRAMAFIC AND RELATED ROCKS, Wyllie, P. J., (Ed.), John Wiley and Sons, New York: New York, p. 212-222.

Hostetler, P. B., et al. ,1966, BRUCITE IN ALPINE SERPENTINITES, American Mineralogist, v. 51, p. 75-98.

Klasner, J. S., 1977, BOUGUER GRAVITY ANOMALY MAP, BARAGA-DEAD RIVER BASINS AREA, NORTHERN MICHIGAN, United States Geological Survey Open-File Report no. 77-746.

___, and W. F. Cannon, 1974,
GEOLOGIC INTERPRETATION OF GRAVITY PROFILES IN THE WESTERN MARQUETTE DISTRICT, NORTHERN MICHIGAN,
Geological Society of America Bulletin, v. 85, p. 213-218.

___, et al., 1977,
THE YELLOW DOG PERIDOTITE AND A POSSIBLE BURIED IGNEOUS COMPLEX OF LOWER KEWEENAWAN AGE IN THE NORTHERN PENINSULA OF MICHIGAN,
United States Geological Survey Open-File Report no. 77-93, 49 p.

___, et al., 1978,
BOUGUER GRAVITY ANOMALY MAP OF THE NORTHERN MICHIGAN-LAKE SUPERIOR REGION,
United States Geological Survey Open-File Report no. 78-211.

Morris, W. J., 1977,
GEOCHEMISTRY AND ORIGIN OF THE YELLOW DOG PLAINS PERIDOTITE, MARQUETTE COUNTY, MICHIGAN,
Master of Science Thesis, Michigan State University, East Lansing, Michigan.

Naldrett, A. J., and L. J. Cabri, 1976,
ULTRAMAFIC AND RELATED MAFIC ROCKS: THEIR CLASSIFICATION AND GENESIS WITH SPECIAL REFERENCE TO THE CONCENTRATION OF NICKEL SULFIDE AND PLATINUM-GROUP ELEMENTS,
Economic Geology, v. 71, p. 1131-1158.

Nesbitt, R. W., 1971,
SKELETAL CRYSTAL FORMS IN THE ULTRAMAFIC ROCKS OF THE YILGARN BLOCK, WESTERN AUSTRALIA: EVIDENCE FOR AN ARCHEAN ULTRAMAFIC LIQUID,
Geological Society of Australia Special Publication 3, p. 331-347.

O'Hara, M. J., 1967,
MINERAL FACIES IN ULTRABASIC ROCKS, In; ULTRAMAFIC AND RELATED ROCKS,
Wyllie, P. J., (Ed.), John Wiley and Sons, New York: New York, p. 7-18.

Pyke, D. R., A. J. Naldrett, and O. R. Eckstrand, 1973,
ARCHEAN ULTRAMAFIC FLOWS IN MUNRO TOWNSHIP, ONTARIO,
Geological Society of America Bulletin, v. 84, p. 955-978.

Talwani, M., J. L. Worzel, and M. G. Landisman, 1959,
RAPID GRAVITY COMPUTATIONS FOR TWO-DIMENSIONAL BODIES WITH APPLICATION TO THE MENDOCINO SUBMARINE FRACTURE ZONE,
Journal of Geophysical Research, v. 64, p. 49-59.

Thayer, T. P., 1960,
SOME CRITICAL DIFFERENCES BETWEEN ALPINE - TYPE AND STRATIFORM PERIDOTITE - GABBRO COMPLEXES,
21st International Geological Congress, Copenhagen, Reports, pt. 13, p. 247-259.

Trow, J., 1978a,
PRELIMINARY GEOLOGIC DATA -- DIAMOND - DRILLING FOR GEOLOGIC INFORMATION IN THE MIDDLE PRECAMBRIAN BASINS IN THE WESTERN PORTION OF NORTHERN MICHIGAN,
Michigan Department of Natural Resources, Geological Survey Open File Report no. DOE OFR 78-1, Prepared for the United States Department of Energy, Project No. 20-77-2132.

___, 1978b,
PRELIMINARY GEOLOGIC DATA -- DIAMOND - DRILLING FOR GEOLOGIC INFORMATION IN THE MIDDLE PRECAMBRIAN BASINS IN THE WESTERN PORTION OF NORTHERN MICHIGAN,
Michigan Department of Natural Resources, Geological Survey Open File Report no. DOE OFR 78-3, Prepared for the United States Department of Energy, Project No. 20-77-2132.

___, 1978c,
PRELIMINARY GEOLOGIC DATA -- DIAMOND - DRILLING FOR GEOLOGIC INFORMATION IN THE MIDDLE PRECAMBRIAN BASINS IN THE WESTERN PORTION OF NORTHERN MICHIGAN,
Michigan Department of Natural Resources, Geological Survey Open File Report no. DOE OFR 78-7, Prepared for the United States Department of Energy, Project No. 20-77-2132.

Turekian, K. K., and K. H. Wedepohl, 1961,
DISTRIBUTION OF THE ELEMENTS IN SOME MAJOR UNITS OF THE EARTH'S CRUST,
Geological Society of America Bulletin, v. 72, p. 175-192.

Vinogradov, A. P., 1962,
AVERAGE CONTENTS OF CHEMICAL ELEMENTS IN THE PRINCIPAL TYPES OF IGNEOUS ROCKS OF THE EARTH'S CRUST,
Geochemistry no. 7, p. 641-664.

Wedepohl, K. H., 1975,
THE CONTRIBUTIONS OF CHEMICAL DATA TO ASSUMPTIONS ABOUT THE ORIGIN OF MAGMAS FROM THE MANTLE,
Fortschritte der Mineralogie, v. 52, p. 141-172.

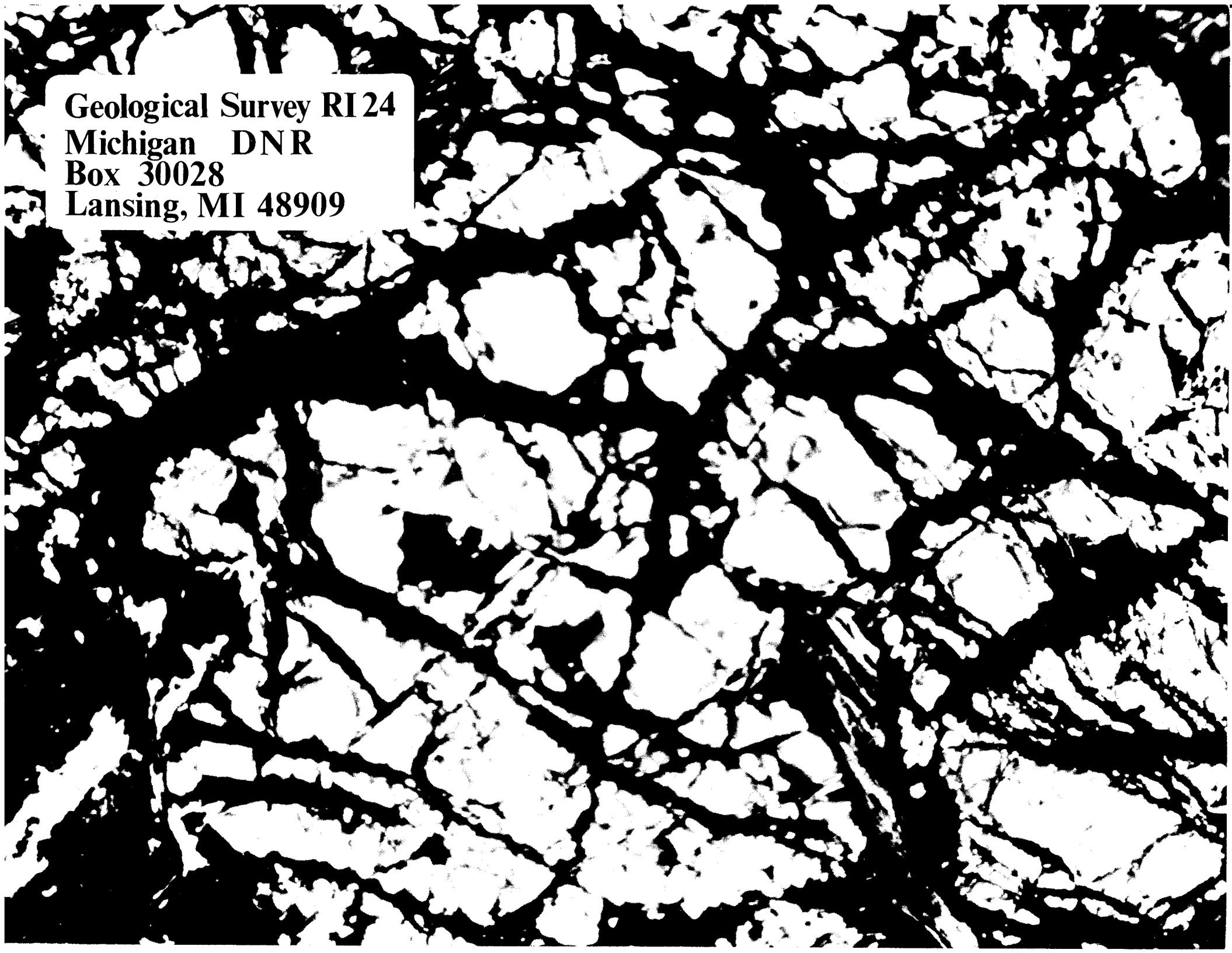
Geological Survey RI 24
Michigan DNR
Box 30028
Lansing, MI 48909